Cellulose (2015) 22:3441–3463
DOI 10.1007/s10570-015-0696-x

ORIGINAL PAPER

Bacteriostatic photocatalytic properties of cotton modified with TiO_2 and TiO_2/aminopropyltriethoxysilane

Brigita Tomšič · Vasko Jovanovski · Boris Orel · Mohor Mihelčič · Janez Kovač · Vojmir Francetič · Barbara Simončič

Received: 8 May 2015 / Accepted: 29 June 2015 / Published online: 26 July 2015

Abstract A new route for the functionalization of cotton fibres with organic–inorganic hybrid materials is proposed using titanium tetraisopropoxide (TiP) and aminopropyltriethoxysilane (APTES). The antimicrobial and photocatalytic activities of the new cotton finishes based on titania and mixed titania/amino-silica hybrids were tested by monitoring the growth of *Escherichia coli* (ATCC 25922) on the surfaces of functionalized fabrics under exposure to UV radiation and in the dark. Transmission electron microscopy revealed the amorphous nature of the hybrids and confirmed their similarity to other bactericidal aminofunctionalized polymers. Attenuated total reflection infrared spectra showed the protonated amino groups of the APTES in the TiP/APTES hybrid and the presence of Si–O–Ti bonding within the sol–gel hybrids between silica and titania by analogy with previous transmission and ATR infrared studies. Several analytical techniques were employed to establish the presence of the TiP and TiP/APTES modified cotton fibres. ATR measurements proved to be a very useful tool to study also the silane/–C–OH interactions between the hybrid materials and the cotton fibres, revealing the presence of covalent (i.e., –Si–O–C–) bonding with the OH functional group of cellulose. The advantages of the cotton finishes were demonstrated by the measured photocatalytic bacteriostatic effect, which persisted even after 15 washings; in contrast, the aminofunctionalized polymeric finishes, only showed a sufficient bacteriostatic effect. Furthermore, the TiP finishes were photocatalytically active, while the TiP/APTES finishes were not. The ultraviolet protective factor, degree of polymerization of the finished cotton samples were also investigated and revealed the suitability of the proposed method.

Keywords Cotton · Titania/silica hybrid coating · Antimicrobial properties · Photocatalytic properties · UV absorption · Washing fastness

B. Tomšič · B. Simončič (✉)
Department of Textiles, Faculty of Natural Sciences and Engineering, University of Ljubljana, Aškerčeva 12, 1000 Ljubljana, Slovenia
e-mail: barbara.simoncic@ntf.uni-lj.si

V. Jovanovski · B. Orel (✉) · M. Mihelčič
National Institute of Chemistry, Hajdrihova 19, 1000 Ljubljana, Slovenia
e-mail: boris.orel@ki.si

M. Mihelčič
Jozef Stefan International Postgraduate School, Jamova cesta 39, 1000 Ljubljana, Slovenia

J. Kovač
Institut Jožef Stefan, Jamova 39, 1000 Ljubljana, Slovenia

V. Francetič
Faculty of Chemistry and Chemical Technology, University of Ljubljana, Ljubljana, Slovenia

Introduction

The use of TiO_2 in textile finishes is attracting interest due to its relatively straightforward immobilization

onto cotton fabrics, enabling the fabrication of cotton fabrics with excellent protection against UV radiation, expressed in a high UV protection factor (UPF) (up to 50) (Saravanan 2007), and its photocatalytic bacteriostatic effects (Matsunaga et al. 1988; Saito et al. 1992; Linsebigler et al. 1995; Fujishima et al. 1999; Qi et al. 2006; Daoud et al. 2005; Wang et al. 2005; Li et al. 2008).

The photocatalytic antibacterial effect is not yet fully understood. According to Matsunaga et al. (Matsunaga et al. 1988), the presence of photogenerated holes on the surface of TiO_2 leads to electron transfer from coenzyme A (intracellular enzyme), inducing oxidation and the formation of dimeric coenzyme A, which decreases respiratory action and causes cell death. However, other mechanisms have also been proposed (Saito et al. 1992; Sunada et al. 1998, 2003; Kiwi and Nadtochenko 2005; Maness et al. 1999; Lu et al. 2003; Nadtochenko et al. 2008). It is now believed that photocatalytically reactive oxygen species (OH*, HO_2*, and O_2^{-}* radicals) further attack polyunsaturated phospholipids, causing the cell membrane breakdown and the failure of vital functions, such as the above-mentioned respiratory activity failure. As reported by Lu et al. (2003) in AFM and SEM studies (Liu et al. 2010), the photocatalytic action of TiO_2 significantly changes the surfaces of cells, modifying their shapes from rod-like to elliptical. The results show that the peroxidation of lipids also induces DNA damage and disruption of the cell membrane morphology due to the electron transport chain (Kumar et al. 2011).

One of the advantages of the TiO_2 nanoparticle coatings lies in the fact that they also kill the bacteria cells in the dark, and this action can be strongly influenced by the functionalization of the particle surfaces. For example, Thevenod et al. (2008) showed that the killing of the tumour cells is significantly enhanced when the TiO_2 nanoparticles were functionalized with organic molecules containing $-OH$, $-NH_2$ and $-COOH$ groups. $-NH_2$ groups are the most effective, in agreement with the findings of Li et al. (2005) and Nur (2006), who demonstrated the synergetic bactericidal effects of TiO_2 nanoparticles in the presence of aminosilanes. Similar effect was observed by Čepin et al. (2015) when nanocrystalline ZnO was modified with various amino-silanes and ionic liquid-silanes.

The antimicrobial effects of amino groups led to the development of antibacterial polymeric systems (Timofeeva and Kleshcheva 2011) with protonated primary or secondary/tertiary amine groups. Quaternary ammonium groups attached on various polymers (i.e., polymers of 3-(trimethoxysilyl)-propyldimethyloctadecyl ammonium chloride (Isquith et al. 1972; Tomšič et al. 2011; Simončič et al. 2012), copolymers of N-vinylpyrrolidone with (2-methacryloxyethyl)-triethylammonium halides (Panarin et al. 1971), poly(2-alkyl-1,3-oxazoline)s (alkyl = methyl, ethyl) with terminal quaternary ammonium groups (Waschinski and Tiller 2005) were the most efficient. Also relevant to this study is Milovic et al.'s (2005) demonstration that glass slides coated with aminopropyltriethoxysilane covalently derivatized with N-hexyl,methyl-polyethylenimine killed bacteria over the course of many successive generations. The killing effect of the corresponding coating has been attributed to the rupturing of bacterial cell membranes after contact with the amino functionalized polymeric chains.

Here, titanium tetraisopropoxide (TiP) precursor both alone and in combination with aminopropyltriethoxysilane (APTES) was selected and used for the preparation of TiO_2 and mixed TiP/APTES cotton fabric finishes. The sol–gel TiP/APTES hybrid finishes resemble aminofunctionalized polymeric systems in many aspects. Namely, TiP/APTES hybrids belong to a class of organic–inorganic hybrid materials that have been extensively studied in our laboratory in the past (Vince et al. 2006; Fir et al. 2007; Jerman et al. 2008; Vilčnik et al. 2009; Koželj et al. 2009; Čolović et al. 2011; Jerman et al. 2012; Simončič et al. 2014; Vasiljević et al. 2014). In the TiP/APTES hybrids studied here, the TiP and APTES acted as sol–gel network formers, while the amino groups of the APTES (the organic part of the hybrid) imparted the hybrid with bactericidal properties. To mimic the bactericidal aminofunctionalized polymeric systems as much as possible (Timofeeva and Kleshcheva 2011), the TiP/APTES hybrids were intentionally kept amorphous. To avoid the formation of crystalline titania within the TiP/APTES hybrid (Brooks and Moore 2000; Vuk et al. 2006; Moulder et al. 1995), favourably low processing temperatures ($\sim$100 °C) were used for the fabrication of the cotton finishes. In this way, the presence of TiO_2 particles

may lead to the loss of the Si–O–Ti inter phase bonds within the nanocomposite and between the titania nanoparticles and the cotton. Both of these interactions are important for the washing fastness of the functionalized cotton fabrics.

The aim was to produce amorphous coatings in a single step at temperatures below 100 °C by avoiding any post-deposition heat treatment. Inspection of the synthetic procedures revealed that the autoclaving of sol–gel or metal salt TiO_2 precursors at controlled water/ethanol pressures (Langlet et al. 2002, 2003) and the fabrication of TiO_2 suspensions at elevated temperatures from various acidic or basic aqueous solutions (Bacsa and Grätzel 1996; Kumar et al. 1994; Chemseddine and Moritz 1999; Yun et al. 2004) were not appropriate, leading us to focus on hot water treatment procedures (Kotani et al. 2000; Matsuda et al. 2000, 2003). The hot water treatment of cotton seemingly gives excellent results and enables the deposition of transparent anatase nanocomposite films on PET, PC, acrylic resin substrates and cotton fabrics. The corresponding finishes (Kotani et al. 2000; Matsuda et al. 2003) were mostly obtained by immersing cotton in hot water solutions of titania precursors followed by treatment at 90 °C to accelerate the condensation into nanocrystalline TiO_2. We simplified the titania formation process by soaking the cotton in the ethanolic solutions of TiP and TiP/APTES precursors and then immersing the soaked cotton fabrics in boiling water for several minutes. This procedure was not only faster, because of the elimination of the post-deposition treatment of cotton at 90 °C, but was also performed at neutral pH, avoiding the depolymerization of cotton fabrics that occurs at low pH values (Langlet et al. 2002; Mahltig et al. 2007). It should be noted that the application process is cost-effective and has practical potential because of cheap precursors, simplicity of the implementation process and the use of conventional equipment.

In addition to the main aim of this study, which is to demonstrate the bactericidal photocatalytic action of sol–gel TiP/APTES hybrid, the structural properties of these modifications were studied in detail. First, they were determined using attenuated total reflection (ATR) infrared spectroscopy and by focusing on the hydrolysis and condensation of the precursor solution under the same conditions as employed during the modification of the cotton fabric. Our main interest was to establish the presence of Si–O–Ti bonds within the sol–gel hybrids between silica and titania by analogy with previous infrared transmission (Schraml-Marth et al. 1992) and ATR studies (Aizawa et al. 1991) performed on silane coatings on titania particles (Puzenat and Pichat 2003; Mihelčič et al. 2014). In addition, the existence of SiOH bands and Si–O–Si bonds (Mihelčič et al. 2014; Brinker and Scherer 1990; Arkles and Larson 2004) in the hybrids and the presence of protonated amino groups in APTES (Bellamy 1954) were investigated using ATR. TEM micrographs were used to reveal the amorphous nature of the hybrids to confirm their similarity to other bactericidal aminofunctionalized polymeric systems (Timofeeva and Kleshcheva 2011).

The presence of TiP and TiP/APTES hybrids on cotton fibres was established by SEM, EDX, XPS and ATR infrared spectroscopic measurements. The latter technique has been extensively employed for the identification of vibrational modes of cellulose and its derivatives (Tsuboi 1957; Maréchal and Chanzy 2000; Chung et al. 2004; Hinterstoisser et al. 2001; Hinterstoisser and Salmén 1999) with different moisture contents (Hofstetter et al. 2006; Olsson and Salmén 2004; Tshabalala et al. 2003) and in the presence of various (mainly silane-based) coatings (Castellano et al. 2004; Xie et al. 2010; Abdelmouleh et al. 2002) and other coupling agents (Rasmussen et al. 2014a), providing a useful platform for investigations of adsorption (Abdelmouleh et al. 2002) and the silane/–C–OH interactions between the coatings and the cotton fibres (Castellano et al. 2004). Investigations oriented to reveal covalent bonding between silane with the OH functionality of cellulose (i.e., –Si–O–C– bonds) are rare (Radetić 2013), and most authors have preferred to focus on the effects of different finishes on the properties of the fabric (Daniels and Francis 1998; Ku et al. 2011) rather than the cellulose/silane interactions. The main emphasis has been to determine the type of bonding between the hybrids and the cotton and the identification of the hybrid anchoring sites on the cellulose via the formation of Si–O–C covalent bonds.

In addition to the structural studies of the cotton finishes, we devoted a great amount of effort to the investigation of the washing fastness of the cotton finishes by TG measurements, to establish the

correlation of the washing fastness with the changes of the UZF values and the degree of polymerization (DP). Finally, the antimicrobial photocatalytic activities of TiP- and TiP/APTES-modified cotton fabric were quantitatively determined by antimicrobial testing with and without UV illumination and correlated to the photocatalytic activities of the TiP and TiP/APTES cotton finishes.

Experimental

Materials

Titanium tetraisopropoxide, $Ti(iOPr)_4$ (TiP) (Aldrich), aminopropyltriethoxysilane (APTES) (ABCR) and absolute isopropanol (Aldrich) were used for the preparation of the nanosols.

Plain-woven 100 % cotton fabric with a mass of 162 g/m^2 was used in the experiments as the substrate. In the pre-treatment process, the fabric was bleached in an H_2O_2 bath, mercerized in NaOH solution and neutralized with dilute CH_3COOH.

Application of the nanosols

For the impregnation of the cotton, three different nanosols, i.e., TiP, APTES and TiP/APTES, were prepared at room temperature. The TiP sol was prepared by mixing $Ti(iOPr)_4$ in isopropanol to a concentration of 5 %. The same procedure was used for the preparation of the APTES sol, except that APTES was used instead of $Ti(iOPr)_4$. The TiP/APTES sol was prepared by mixing $Ti(iOPr)_4$ and APTES in isopropanol to a concentration of 10 %. The molar ratio of $[Ti(iOPr)_4]$:APTES was set to 1:2. Prior to use, the solutions were vigorously stirred for a few minutes. Impregnation of the cotton was achieved by overnight immersion in the precursor solutions at room temperature. The samples were then squeezed by a wet-pick up of 100 %, dipped in boiling water for a few minutes and air-dried.

For the spectrophotometric measurements, 10 % TiP/APTES sols were prepared using various $Ti(iOPr)_4$:APTES ratios (Ti:Si = 1:1, 3:4, 1:1.5, 1:2 and 1:2.5), applied to Si wafers using the dip coating technique and exposed to boiling water steam for specified durations to simulate hydrolysis and the conditions to which the cotton substrates were exposed during the application process. In addition, 5 % sols with one component (either TiP or APTES) were applied to Si wafers using the same procedure.

Washing procedure

The washing fastness of the cotton coatings was tested according to the ISO 105-C01:1989(E) standard method using a Launder-ometer. The samples were treated for 30 min at 40 °C in an ionic soap solution of ECE phosphate reference detergent (B) (SDC Enterprises Limited, United Kingdom) with a concentration of 5 g/l at pH 7, resulting in a liquor ratio of 1:50. The washing procedure was repeated for 20 cycles.

Measurement techniques

Transmission electron microscopy (TEM) micrographs were obtained on a JEOL JEM-2100 high-resolution transmission electron microscope (HR-TEM) operating at 200 keV.

Energy dispersive X-ray spectroscopy (EDX) measurements were performed on a JEOL JED-2300T EDS system with high energy resolution and high sensitivity.

Scanning electron microscopy (SEM) measurements were conducted on a Supra 35 VP FE-SEM (Carl Zeiss).

The presence of the hybrid modifications in the cotton fibres was assessed using a Perkin-Elmer System 2000 IR spectrophotometer equipped with an ATR cell (SpectraTech) with a diamond crystal (n = 2.0). The spectra were recorded over the range 4000–370 cm^{-1}.

X-ray photoelectron spectroscopy (XPS or ESCA) was applied to investigate the chemical statuses of the elements on the surface of the sol–gel coatings. The analysis was performed using a XPS spectrometer produced by Physical Electronics Inc., model TFA XPS. An Al K_α monochromatized X-ray source (200 W) was used. The energy of the X-ray beam was 1486.7 eV. The analysed area was 0.4 mm in diameter, and the signal during the XPS analysis corresponded to a depth of up to 6 nm from the surface layer. The sample charging during the XPS analysis was compensated by a low-energy electron gun-neutralizer. XPS method is sensitive for all elements except H and He can't be detected.

The UV blocking properties of the modified cotton fabric were measured according to the American standard method AATCC 183-2000 using a Varian Cary 1E UV–Vis spectrophotometer.

The antibacterial assessments of TiP, APTES and TiP/APTES-coated cotton samples washed 0, 1 and 10 times were performed using the bacterium *Escherichia coli* (ATCC 25922) according to the AATCC 100-1999 standard method. For the inoculation of the samples, a bacterial suspension with a concentration of 10^5 colony-forming units per ml (CFU/ml) was used. The bacterial growth reduction, R, which is a measure of the bactericidal activity of the studied samples, was determined according to the following equation:

$$R = \frac{B - A}{B} \times 100(\%) \quad (1)$$

where A denotes the number of CFUs that survived 24 h of contact with the studied sample and B denotes the number of CFUs at the beginning of the experiment. The values of A and B used in Eq. 1 were the averages of six counts according to the agar plate counting method. The experiments were performed with and without UV illumination. The UV black light (HQV 125, Osram), with the emission range of 300–400 nm and dimensions of 170 mm in length and 15 mm in diameter, was placed approximately 200 mm above the samples.

The fibre damage due to the photocatalytic activity of the TiP-based finishes was measured viscosimetrically using an Oswald shear dilution viscometer. In addition, the DP of the TiP-coated and uncoated samples was determined. Cuoxam, a solution of cupric hydroxide in aqueous ammonia, $[Cu(NH_3)_4](OH)_2$, was used as the solvent.

The photocatalytic activities of the TiP and TiP/APTES-coated cotton samples were assessed by monitoring the degradation of the colour marker and the dye bromophenol blue, (3′,3″,5′,5″-tetrabromophenolsulfonphthalein) (BPB), (Sigma Aldrich) after the exposure of the dyed fabric samples to artificial light at 65 ± 2 % relative humidity and 20 ± 1 °C using a Xenotest Alpha instrument (Atlas, USA) equipped with a xenon lamp with an adjustable radiation power region 0.8–2.5 kVA and an expanded range of radiation (300–400 nm). Each sample (60 mm × 40 mm) was dyed by 1-min immersion in 25 ml of a 0.04 % water solution of BPB dried at room temperature in the dark for 24 h. The dyed samples were placed in a sample holder and set in the exposure chamber in a vertical position for 30, 60, 90 and 120 min. After illumination, an assessment of the degradation of the dyestuff was performed using the reflectance measurements, R, of the studied samples on a Datacolor Spectraflash SF 600 spectrophotometer using D 65/10° light. For each sample, ten measurements of the R-value were obtained, and the corresponding K/S values were calculated according to the Kubelka–Munk equation (Zollinger 1991):

$$\frac{K}{S} = \frac{(1 - R)^2}{2R} \quad (2)$$

where K/S is the ratio of the coefficient of light absorption (K) to the coefficient of light scattering (S) and R is the reflectance at the maximum absorption wavelength determined at 610 nm. The mean K/S value was then determined.

Based on the K/S values, the dyestuff degradation was determined according to Colleoni (Colleoni et al. 2012):

$$\text{Dyestuff degradation} = \left(1 - \frac{\left(\frac{K}{S}\right)_i - \left(\frac{K}{S}\right)_{UD}}{\left(\frac{K}{S}\right)_0 - \left(\frac{K}{S}\right)_{UD}}\right) \cdot 100(\%) \quad (3)$$

where $(K/S)_{UD}$ is the K/S value of the undyed sample, $(K/S)_0$ is the K/S value of the dyed sample before illumination and $(K/S)_i$ is the K/S value of the sample after illumination for a given time.

Thermogravimetric analysis (TGA) was performed on a Mettler Toledo TGA/SDTA 851^e instrument. The TGA curves were measured from 30 to 800 °C in a nitrogen atmosphere at a heating rate of 10 °C/min.

Results and discussion

SEM, XPS and TEM measurements

SEM measurements

The morphological changes in the cotton fibres after the modification with TiP and TiP/APTES were studied using SEM (Fig. 1). Compared to the surfaces of the untreated cotton fibres, treatment with TiP caused the fibre surface to become rough, with barely detectable particles, suggesting their uneven

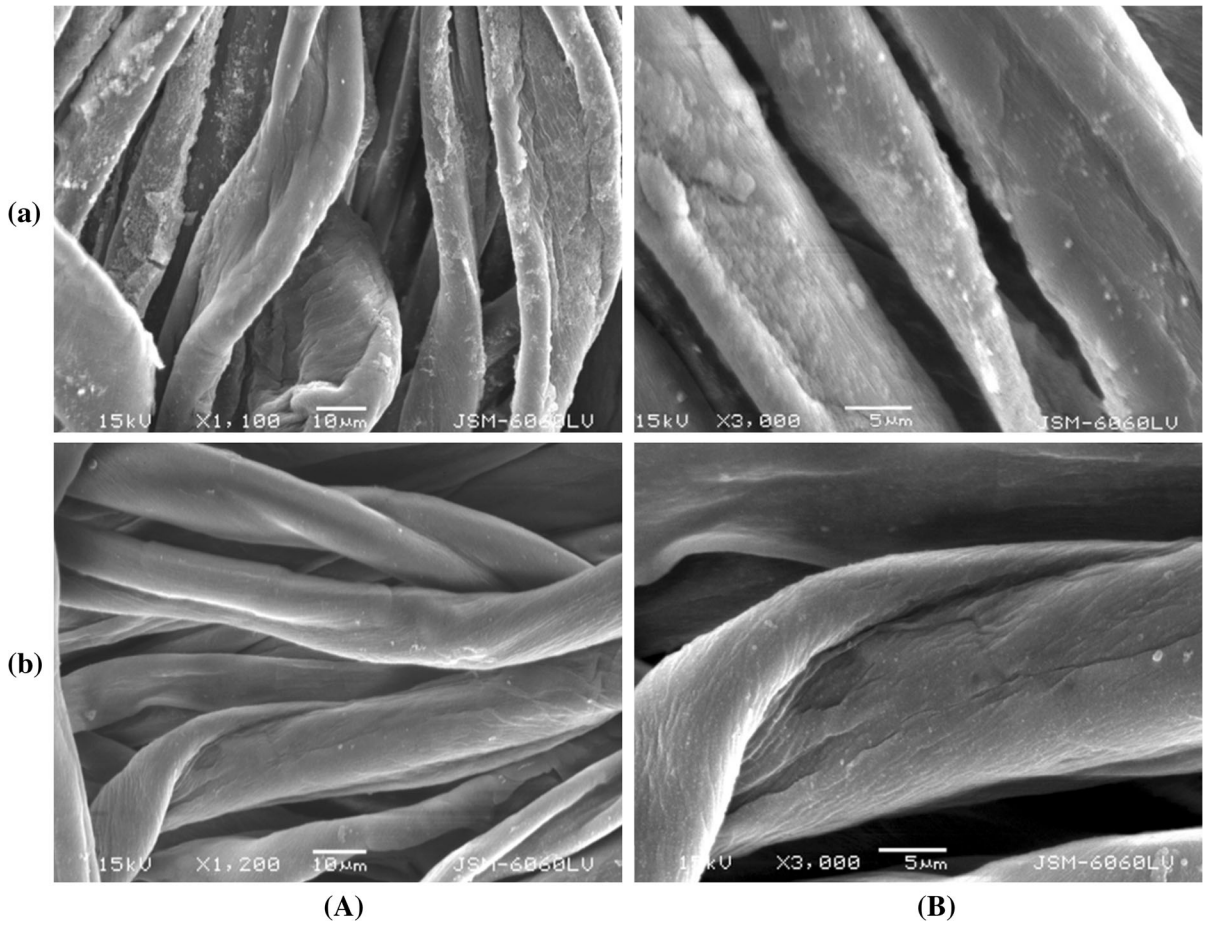

Fig. 1 SEM images of the TiP-coated cotton (**a**) and TiP/APTES-coated cotton (**b**) fibres taking at lower (**A**) and higher (**B**) magnification

distribution. In contrast, the surfaces of the TiP/APTES-treated cotton fibres were smooth, indicating a homogeneous layer without any detectable particles, suggesting an amorphous finish. The estimated size of the particles in the TP finishes was less than 1 µm. Cross-sectional SEM images of the TiP-coated fibres and the carbon, oxygen and titanium elemental contents were obtained. As expected, the results confirmed the presence of titanium on the fibre surface (points 1 and 6 in Fig. 2), but surprisingly, a greater amount of titanium was found in the inner part of the fibre (point 3 in Fig. 2), which clearly indicated that TiP deposition occurred not only on the surface of the fibres, as previously expected, but mainly in the bulk of the cotton fibres. Due to the penetration of the electron beam inside the cotton fibres, the cotton below the cross-cut visible in Fig. 1 could contribute to the observed EDX signal.

XPS measurements of cotton finishes

XPS analysis of the cotton fabrics with applied hybrids was performed to provide information about the surface compositions as well as the chemical environments and bonding of chemical species to the surface. The XPS spectrum of cellulose has been studied by Belgacem et al. (1995), while the XPS spectra of cotton fabrics with applied silane-based coatings have been studied by Mihailovic et al. (2011) and Abdelmouleh et al. (2002). Valades-Gonzales et al. (1999) studied henéquen fibres, which contain hemicellulose, lignin and waxes. The double peaks at 102 eV (Si 2p)

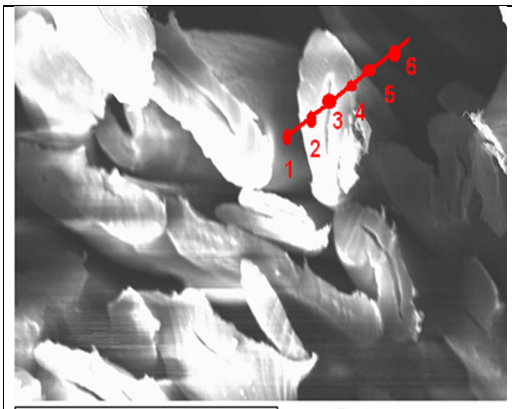

point	Elemental content (A%)		
	C	O	Ti
1	48.24	40.91	5.82
2	49.00	30.94	7.33
3	64.89	33.59	0.44
4	69.40	29.93	0.40
5	71.08	28.41	0.38
6	63.38	31.26	5.36

Fig. 2 Cross section of the TiP/cotton fibre and the elemental content of C, O and Ti at different measuring points

and 150 eV (Si 2s) indicated the presence of silicon atoms, while the C 1s peak at ~288 eV allowed the identification of the attachment of the silane coatings on the fibre surfaces. The C 1s peak splits into peaks at 288, 287 and 285.5 eV (Valadez-Gonzalez et al. 1999) indicating the presence of more than just one compound type bonding. The increase in the intensity of the peak at 285.5 eV relative to the peak at 288 eV (Abdelmouleh et al. 2002), which intensity increased due to the presence of methylene groups of silane, has been attributed to the C–O–Si bond on the cotton fibre surface. The variation in the C 1s peaks upon the application of silane is accompanied by a corresponding decrease in the surface O/C ratio.

Our XPS investigations (Fig. 3) showed that the chemical interaction of the TiP and TiP/APTES hybrids with the cellulose fibres decreased the C content, increased the O content, and led to the appearance of signals from Ti, Si, and N. The results revealed that the cellulose fibres treated with TiP and those treated with TiP/APTES contained Ti in significant amounts (9.7 and 7.0 %, respectively). Furthermore, TiP/APTES contained more N than TiP, and the latter contained a small amount of Si, which we attributed to impurities.

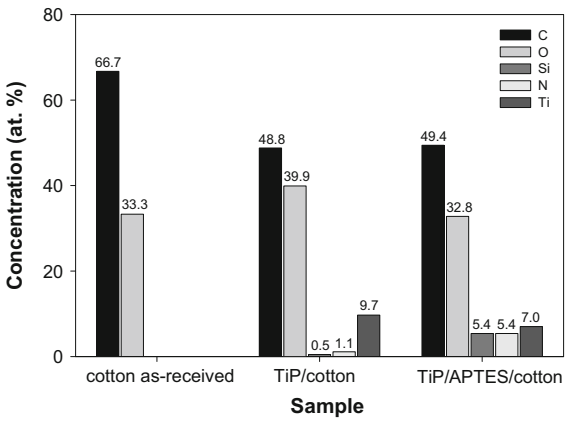

Fig. 3 Surface composition of cotton as-received and cotton treated with TiP and TiP/APTES hybrids

As shown in Fig. 4, two components could be identified in the XPS spectrum of O 1s (Fig. 4a). We attributed the peak at 530.0 eV to the oxygen lattice atoms in the TiO_2 structure, but the peak at 532.5 eV could be assigned to the OH, C–O, Si–O, and H_2O groups, all of which existed in the TiP/APTES cotton coatings and untreated cotton. Expectedly, the XPS spectrum of Ti (Fig. 4b) is a doublet structure consisting of Ti $2p_{3/2}$ and Ti $2p_{1/2}$ peaks separated by 5.5 eV. The Ti $2p_{3/2}$ peak is at ~458.7 eV and can be assigned to the Ti(4+) oxidation state in the TiO_2 structure.

Regarding the identification of the covalent Si–O–C bonds for the TiP/APTES hybrids with cotton, the O 1s spectra were less persuasive than the C 1s spectra obtained for the untreated samples (Fig. 4c) and the samples treated with TiP/APTES (Fig. 4d). For the untreated cotton, the C 1s spectrum consists of typical cellulose components, such as the C–OH peak at 286.4 eV, which is due to the characteristic C–OH bonds for cellulose; the peak at 285.0 eV, associated with the C–C/C–H bonds originating from either the lignin on the surface or adventitious carbon surface species; and the small peak at 288.1 eV, which is due to the C=O and O–C–O bonds in cellulose molecules (Fig. 4c).

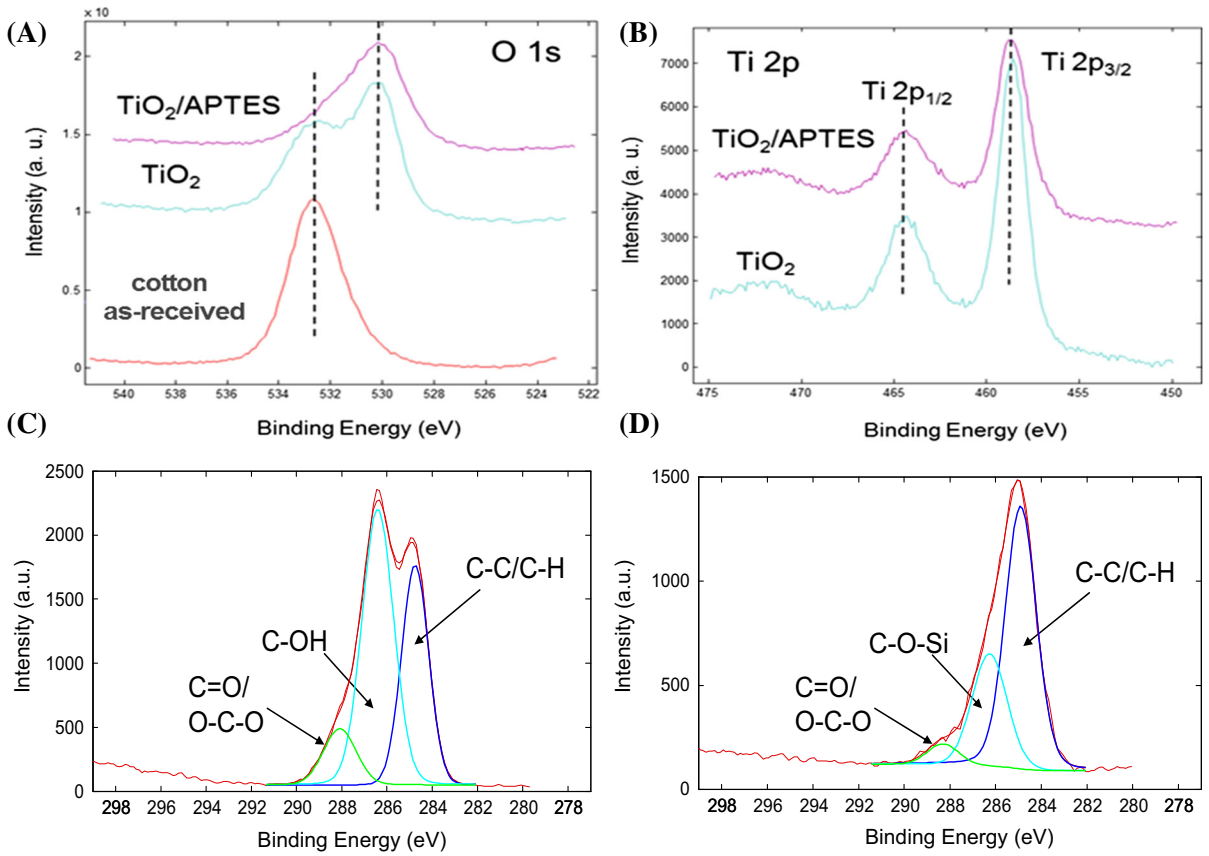

Fig. 4 The XPS O 1s (**a**) and Ti 2p (**b**) spectra of cotton as-received, TiP/cotton and TiP/APTES/cotton; and the XPS C 1s spectra of cotton as-received (**c**) and TiP/APTES/cotton (**d**)

The C 1s spectrum obtained after treating cotton with TiP/APTES (Fig. 4d) differed greatly from that of the untreated cotton. The main peak at 285.0 eV was due to the C–C/C–H bonds in the APTES structure, and the peak at 286.3 eV may be due to the C–O–Si bonds between the C atoms from the cellulose structure and the Si–O part of the silane molecule. There is also a small peak at 288.1 eV due to the C=O/O–C–O bonds. Because the signal during the XPS analyses is coming from the topmost 2–5 nm of the sample, the presence of the C–O–Si bonds in the XPS spectrum of the treated sample may indicate a reaction between the cellulose and the APTES molecules.

TEM and XRD measurements

Weakly expressed and barely observed TiO_2 particles on TiP/cotton fibres and the complete absence of any particles on the surfaces of the TiP/APTES cotton finishes motivated us to perform TEM measurement of TiP and TiP/APTES fine powders collected from the boiling water into which the precursor solutions were poured. The results revealed that the TiO_2 powder was highly agglomerated anatase with particle sizes of 5–10 nm, while the TiP/APTES powder was amorphous (Fig. 5). These results indicated that the TiP/APTES hybrids applied on cotton were likely to be amorphous and, in this respect, resemble the structures of the aminofunctionalized polymeric systems. As expected, the presence of TiP, despite its nanocrystalline form was not detected from the diffraction spectra of TiP/cotton samples (Fig. 6) because the amount of TiP was only 1.93 % w/w (Fig. 17a), which was too low compared to the detectable limit of small molecules (~8 %) that are crystalline and are mixed with cellulose. Even though the same argument could be applied also for TiP/APTES, the absence of this finis was directly consequence of its amorphous state.

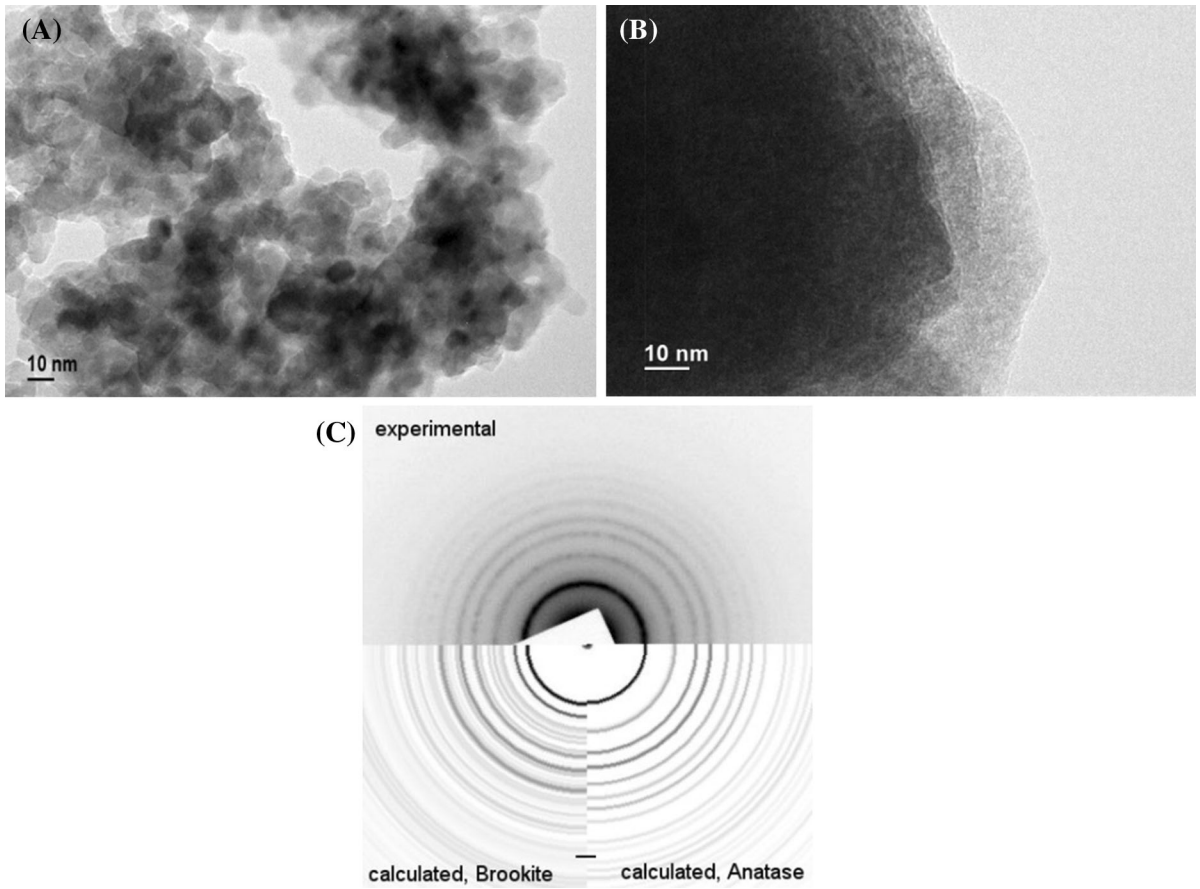

Fig. 5 TEM images of TiP (**a**) and TiP/APTES (**b**) powders obtained in the same way as used for the treatment of cotton and the corresponding interference fringes of anatase structure (**c**) of the TiP nanoparticles

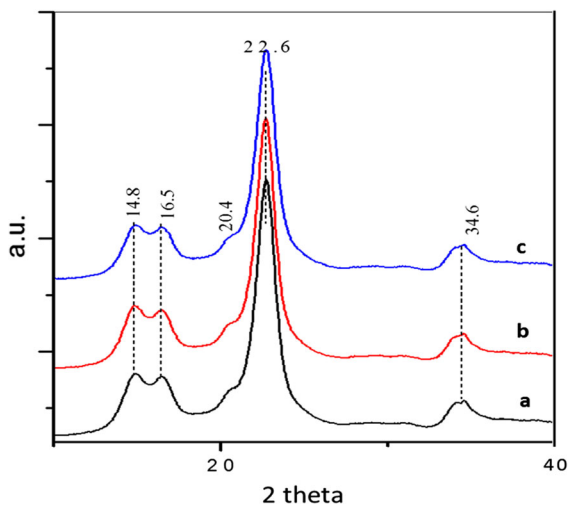

Fig. 6 XRD spectra of the studied cotton samples: cotton as-received (**a**), TiP/cotton (**b**) and APTES/TiP/cotton (**c**)

Properties of the finished cotton fabrics

UV absorption of the fabrics

The UV absorption study of the modified fabric samples (Table 1) revealed high UPFs, i.e., 31 for the TiP- and 18 for the TiP/APTES-coated samples, compared to a low UPF of 5 for untreated cotton. Lower UPF rating of the TiP/APTES-coated sample was attributed to the amorphous structure of the TiP/APTES hybrid coating in contrast to anatase TiP. The total hemispherical transmission of both coated samples was very low in the UV-A region but increased considerably in the UV-B region. This effect was attributed to the absorption of the TiP coating stemming from the anatase band gap energy of approximately $E_{gap/TiO2} \sim 3.2$ eV (Mahltig et al. 2005).

Table 1 Ultraviolet protective factor (UPF) and transmission in the UV-A and UV-B region of the studied samples before and after repeated washings

Sample	Washing cycles	UPF_{mean}	$T(UV\text{-}A)_{mean}$ (%)	$T(UV\text{-}B)_{mean}$ (%)
Cotton as-received	/	5.4	16.3	22.9
TiP/cotton	0	31.1	1.9	13.6
	1	35.8	1.6	12.4
	5	30.6	1.9	12.9
	10	30.0	2.0	12.9
	20	32.8	1.0	10.9
TiP/APTES/cotton	0	18.2	2.9	18.0
	1	20.5	2.4	16.5
	5	30.9	1.4	13.4
	10	28.4	1.6	13.4
	20	26.9	1.7	14.1

The increase of the UPF rating observed for both washed coated samples was hardly to explain, without assuming that during washings the cotton fibres formed lumps due to the shrinkage and compaction of the weft and warp yarns, which excessively scattered and absorbed light. However, the main reason for the retention high UV blocking capacity of finishes we attributed to the to the formation of covalent bonding resulting from a dehydration reaction between the hydroxyl groups of TiO_2 and SiO_2 and hydroxyl groups of cotton (Radetić 2013).

Figure 7a, b show hemispherical total reflection (TR) and hemispherical total transmission (TT) spectra of the untreated cotton sample, the untreated cotton sample soaked overnight in EtOH and then dipped in boiling water as well as the cotton samples coated with TiP and TiP/APTES. The absorption (A) spectra derived from the TR and TT spectra using the relation $[A = 1 - (TT + TR)]$ are shown in Fig. 7c. Inspection of the corresponding spectra revealed that the cotton sample treated in EtOH reflected (Fig. 7a) and transmitted (Fig. 7b) more UV radiation than the coated cotton samples, which proved its low absorption in the spectral region of $\lambda < 500$ nm (Fig. 7c). In contrast, the cotton samples coated with TiP and TiP/APTES strongly absorbed UV radiation up to 450 nm. These samples became non-absorbing in the 550–1200 nm spectral region, but their NIR absorption, which is interrupted by typical cotton absorptions, gradually increased. The TiP and TiP/APTES coatings were not exceptionally good UV absorbers compared to other cotton coatings in which TiO_2 forms a continuous layer on the fibre surface (Langlet et al. 2002).

Photocatalytic antimicrobial properties

The photocatalytic antimicrobial activity of cotton samples modified with TiP and TiP/APTES was quantitatively determined using an antimicrobial test performed in two different ways: with and without UV illumination. It is well known that several reactive oxygen species are generated by the photocatalytic reactions of TiO_2. These reactive species cause oxidation of the membrane lipids leading to the loss of cell viability and cell death (Sunada et al. 2003; Maness et al. 1999; Ibáñez et al. 2003; Hu et al. 2007). Moreover, Kikuchi et al. (1997) proposed that the actual lethal agent was hydrogen peroxide produced from hydroxyl radicals and superoxide anions. Therefore, it is not surprising that, under UV irradiation, the TiP coating showed a 60 % reduction in *E. coli*, which increased to 83 % after the addition of APTES due to the presence of amino groups (Table 2). APTES alone yielded a 52 % reduction in bacteria. The insignificant changes in bacteria growth on the untreated illuminated and not illuminated samples proved that UV irradiation did not add to the antimicrobial effect. The *E. coli* growth reduction of 60 % obtained for the TiP coating was very similar to that observed for TiO_2 powder (P25 Aeroxide, Degussa), which represents an anatase-brookite modification (Kowal et al. 2014), and nanocrystalline titania sol obtained by low-temperature sol–gel synthesis (Galkina et al. 2014). It should be noted that, despite being amorphous, the TiP/APTES hybrid finishes also showed a photocatalytic bacetriostatic effect, which is much more pronounced for crystalline anatase modification than for the

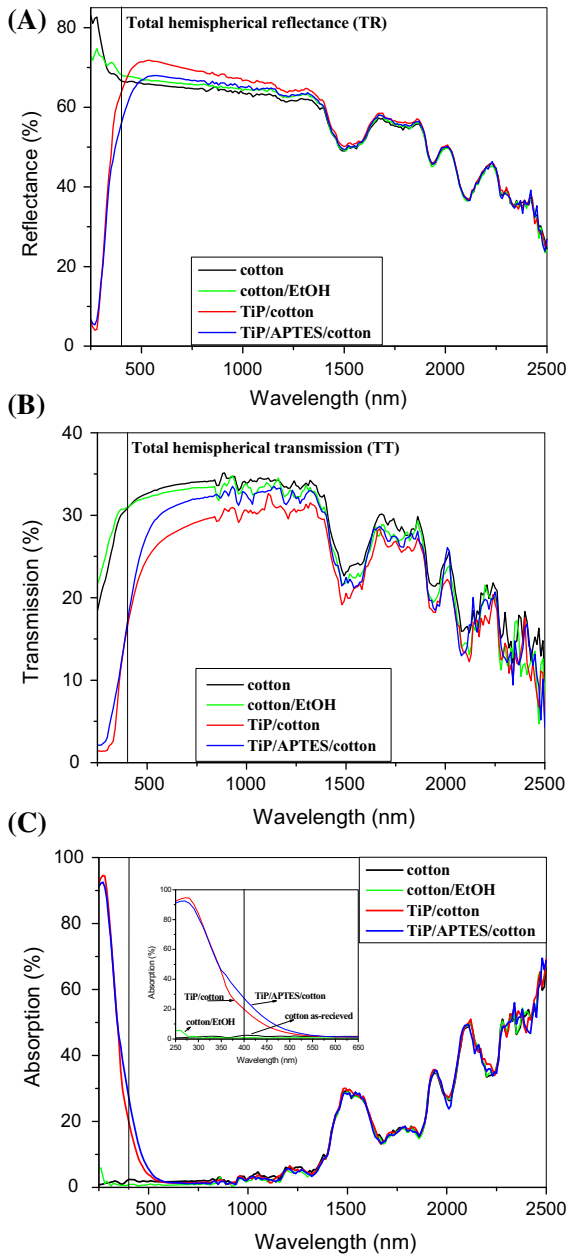

Fig. 7 Total hemispherical reflection (TR), total hemispherical transmission (TT) and absorption spectra of cotton as-received, cotton treated in EtOH (cotton/EtOH) and dipped in boiling water, TiP/cotton and TiP/APTES/cotton samples

amorphous noncrystalline titania coatings according to the literature (Radetic 2013).

The results gathered in Table 2 clearly indicate very good and durable bacteriostatic activities of the TiP and TiP/APTES coatings that were enhanced by UV irradiation. After repeated washings, the bacterial reduction for the TiP coating slightly increased. Meanwhile, the bacterial reduction for the TiP/APTES coating decreased by 10 % after the first washing and then did not change significantly after ten washings. At this point, it must be stressed that one washing in the Lauder-ometer is equivalent to five domestic washings. The APTES coating gave a negative bacterial reduction after the first washing, showing no washing durability, which could be attributed to the loss of the silane from the fibres or, more likely, blocking of the bacteriostatic effect of the amino groups. As expected, the bacterial activity of the TiP and TiP/APTES finishes strongly decreased under dark conditions (i.e., 18 and 51 %) due to the suppressed photocatalytic activity of TiO_2 in both examined coatings.

DP measurements

Photodegradation of the 1,4-β-glucosidic bond of cotton cellulose due to the photocatalytic activity of TiO_2 was studied by the measurement of the DP after different periods of UV illumination. It is well known that free radicals initiate the oxidative degradation of cellulose, which ruptures the (1 → 4) β glycosidic bonds of cellulose macromolecules and thus decreases the DP (Duan and Kasper 2011). Moreover, it has also been proven that, among the reactive species, the decrease in the DP is caused by free hydroxyl radicals, which abstract hydrogen atoms from cellulose molecules to form short-lived cellulose radical species, which then initiate further degradation processes (Fukatsu et al. 1999; Malešič et al. 2005). The results showed (Fig. 8) that, after 96 h of UV illumination, the DP of cellulose in the studied samples did not change significantly, indicating that the degradation process either did not occur to the extent that was measureable by the DP or did not occur at all. This result is in agreement with the poor photocatalytic efficacies of the TiP and TiP/APTES finishes.

Photocatalytic self-cleaning properties

Figure 9 shows the degradation of BPB deposited on the studied samples as a function of the UV exposure time, i.e., 30, 60, 90 and 120 min. Whereas the photodegradation of BPB on unwashed TiP/APTES/cotton and cotton as received as well as on 10 times washed TiP/APTES/cotton and TiP/cotton samples showed similar trend, the degree of the BPB

Table 2 Reduction (R) of bacteria *Escherichia coli* (ATCC 25922) according to the AATCC 100-1999 Standard Method of the studied samples before and after repeated washings, determined under UV illumination of the samples, R_{UV}, and without one, R_0

Sample	Washing cycles	R_{UV} (%)	R_0 (%)
TiP/cotton	0	59.6 ± 5.9	17.5 ± 5.9
	1	56.8 ± 6.3	/[b]
	10	63.1 ± 2.8	/[b]
APTES/cotton	0	51.9 ± 9.2	50.6 ± 1.7
	1	–[a]	/[b]
	10	–[a]	/[b]
TiP/APTES/cotton	0	82.8 ± 2.0	51.6 ± 3.2
	1	73.7 ± 5.1	/[b]
	10	72.2 ± 5.3	/[b]

[a] No reduction of bacteria

[b] Test was not performed

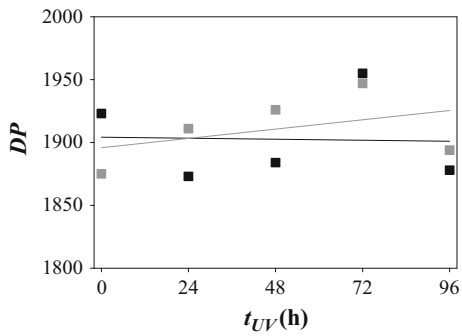

Fig. 8 Degree of polymerisation (DP) of the cotton as-received (*filled square box*) and TiP/cotton (*grey shaded square box*) samples after different time interval of UV illumination, t_{UV}

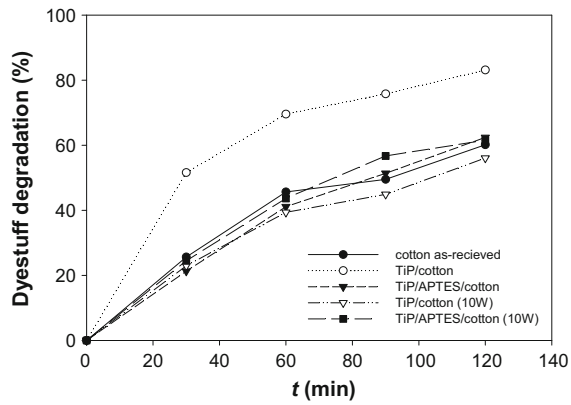

Fig. 9 Degradation of BPB on the cotton as-received, TiP/cotton and TiP/APTES/cotton samples before and after ten consecutive washings (10 W), obtained after different time interval, t, of illumination of the studied samples in Xenotest

photodegradation was significantly higher in the case of the unwashed TiP/cotton sample. BPB was selected deliberately due to the weak light stability stemming from the production of singlet and triplet radical species when illuminated (Subramanian et al. 2014) which after reaction with oxygen, form superoxide, peroxide and hydroxyl radicals (Reactive Oxygen Species) causing the BPB degradation and mineralisation. In the presence of TiP on the dyed cotton sample, the photocatalytic activity of TiO_2 anatase increased the concentration of ROS thus accelerating the BPB photodegradation and discoloration. Results revealed that, a 52 % degradation of BPB was obtained already after only 30 min of UV exposure. Expectedly, the self-cleaning effect became more pronounced by increasing the exposure time, with a 83 % degradation of the dyestuff observed at the end of the experiment. Consecutive washings of the TiP-coated sample caused a gradual decrease in the photocatalytic self-cleaning activity; specifically, the dyestuff degradation rate for the TiP-coated cotton sample washed ten times was equal to that obtained for the bare unfinished cotton. As shown in Fig. 9, the TiP/APTES-coated sample did not possess significant photocatalytic self-cleaning activity, which remained almost the same after ten washings. This lack of activity could be explained by the amorphous nature of the finish and that the amorphous TiO_2 surface was blocked by APTES moiety.

Structural studies: infrared spectral measurements

IR transmission spectra

In a first step, the IR transmission spectra of TiP, APTES and TiP/APTES finishes deposited on Si wafers (see "Experimental" section) were measured, and the vibrational bands signalling the hydrolysis and condensation reactions of the precursors (TiP and APTES) exposed to steam from boiling water were identified and assigned. From the spectra of the APTES coatings, the SiOH, OH···O and Si–O–Si vibrational bands were determined, and the changes attributed to the hydrolysis and condensation reactions were assessed, while the Si–O–Ti bands were assigned from the spectra of the TiP/APTES coatings with various TiP:APTES ratios (Ti:Si = 1:1, 1:2, 3:4, 1:1.5, 1:2.5).

The IR transmission spectra of the as-prepared TiP coatings (Fig. 10a) showed vibrational bands characteristic of TiO_2, which could be due to the increasing absorption below 800 cm^{-1} (Vuk et al. 2005, 2006). The APTES (Fig. 10a) spectra showed Si–O–Si bands at 1128 and 1024 cm^{-1}. The band at 930 cm^{-1} was attributed to SiOH (Orel et al. 2005a, b). After heat treatment at 200 °C (1/2 h), the SiOH vanished from the spectra (Fig. 10b), confirming the condensation reactions of APTES. $N–H_2$ stretching bands at 3656 and 3272 cm^{-1} and the corresponding deformational band at 1596 cm^{-1} were observed, while the mode belonging to the protonated amino groups expected at ~1550–1500 cm^{-1} was not observed because of the neutral pH conditions of the APTES sols (Bellamy 1954).

The IR spectra of various TiP/APTES coatings that were hydrolysed and condensed over water steam (Fig. 10a) and then heated at 200 °C (Fig. 10b) revealed the evolution of the bands attributed to the Si–O–Ti modes at 903 cm^{-1} (Schraml-Marth et al. 1992; Aizawa et al. 1991; Puzenat and Pichat 2003; Mihelčič et al. 2014). The position of the corresponding band at 903 cm^{-1} remained practically the same for all Ti:Si ratios (Fig. 10a, b), but the relative intensity of the Si–O–Ti band with respect to the Si–O–Si band at 1034 cm^{-1} was maximal for TiP/APTES when the Ti:Si ratio was equal to 1.33 (Fig. 10b). The strong Si–O–Ti band indicated highly interlinked silica and titania networks and the formation of a dense and compact hybrid (Schraml-Marth et al. 1992; Aizawa et al. 1991).

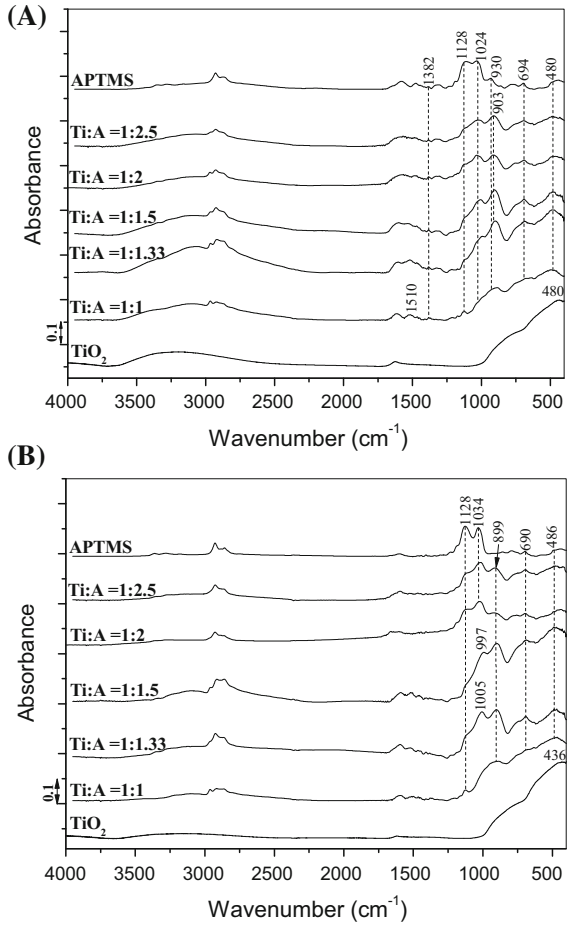

Fig. 10 IR spectra of TiO_2, APTES and various mixtures of TiP/APTES (Ti:A) deposited on a Si-wafer, hydrolysed and partially condensed over water steam (**a**) and then heated at 200 °C (**b**)

The transmission spectra of the TiP/APTES coatings showed a broad OH stretching band at 3051 cm^{-1}, indicating stronger H-bonding (intra and inter) than that found for cellulose (Maréchal and Chanzy 2000; Hinterstoisser and Salmén 1999; Hofstetter et al. 2006), which we inferred from the shift of this band to lower wavenumbers for inter (Hadzi and Orel 1973; Angeloni et al. 1974) and intra (Avbelj et al. 1985) H-bond systems. As expected, the OH stretching band showed a fine structure and redshifted slightly after the heat treatment (Fig. 10a, b).

Another important issue for this study was the establishment of the protonated amino groups, which were identified from the bands at 1550–1533 cm^{-1} and the C–N stretching band at 1275 cm^{-1} in the TiP/APTES spectra. The band at 1550–1500 cm^{-1} did not

appear in the APTES spectra, seemingly because TiP required acidic conditions for the formation of the protonated amino groups (Horner et al. 1992).

ATR IR spectra of the powders

To prevent the misinterpretation of the vibrational bands in the ATR spectra of the cotton finishes, the ATR spectra of the APTES and TiP/APTES powders (see "Experimental" section) (Fig. 11) were recorded and compared to the corresponding transmission spectra (Fig. 12). In the ATR spectra, the bands redshifted and exhibited band shape distortions due to the variable refractive index, which changes in the frequency range of the vibrational band (Vince et al. 2006). This effect is stronger for more intense bands (up to $\Delta\nu \sim -70$ cm^{-1} for the Si–O–Si bands, for example), while the weaker bands showed redshifts in the frequency of only a few cm^{-1} (the SiOH band, for example).

For the APTES powders, Si–O–Si bands appeared at 1070 and 997 cm^{-1} in the ATR spectrum (Fig. 11b) and at 1121 and 1031 cm^{-1} in the transmission spectrum (Fig. 12b). However, weaker SiOH bands were found in the transmission and ATR spectra at nearly the same frequencies i.e., at 929 and 922 cm^{-1}, respectively. As expected, for the TiP samples, the redshifts in the frequency were even greater; in the ATR spectrum (Fig. 11a), no distinct maximum attributed to the Ti–O stretching mode was observed,

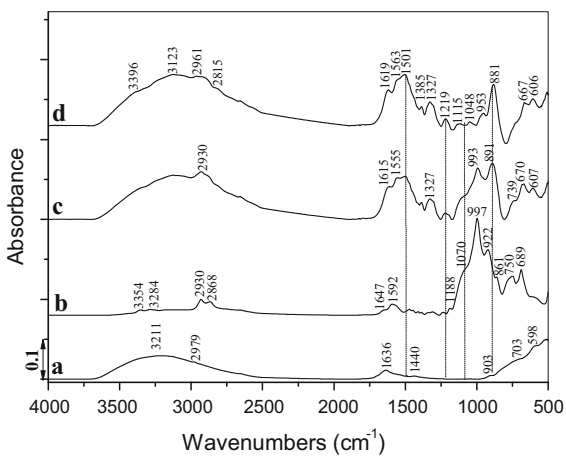

Fig. 11 ATR spectra of TiP (*a*), APTES (*b*) and TiP/APTES (*c*) powders and the subtraction spectrum of APTES from TiP/APTES (*d*)

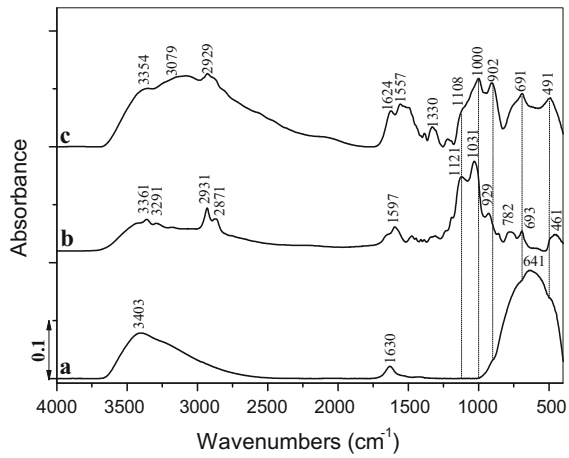

Fig. 12 Transmission spectra of TiP (*a*), APTES (*b*) and TiP/APTES (*c*) powders

but a maximum was clearly seen at 641 cm^{-1} in the transmission spectrum (Fig. 12a) (Vuk et al. 2005, 2006).

In the ATR spectrum of the TiP/APTES (Ti:Si = 1:1.33) powders (Fig. 11c), only one Si–O–Si band was observed at 993 cm^{-1}, while in the corresponding transmission spectrum, two Si–O–Si bands were assigned at 1108 and 1000 cm^{-1} (Fig. 12c). In these spectra, the SiOH and Si–O–Ti bands overlapped, showing only a single, relatively strong and broad band at 891 (ATR) and 902 cm^{-1} (transmission).

Although there was no doubt about the assignment of the Si–O–Ti mode at $\sim$891 cm^{-1} in the ATR spectra, the additional evidence about its mixed mode character was obtained from the (TiP/APTES–APTES) subtraction spectrum (Fig. 11d). The strong positive (881 cm^{-1}) and negative (800 cm^{-1}) bands indicated that the band at 891 cm^{-1} was the superposition of the Si–O–Ti (at 891–920 cm^{-1}) and SiOH bands, which also appeared in this region, as we inferred from the ATR spectrum of the APTES sample (at 922 cm^{-1} in Fig. 11b).

The strong OH stretching band centred at $\sim$3211 cm^{-1} in the ATR spectrum of TiP (Fig. 11a) and at 3123 cm^{-1} in the (TiP/APTES–APTES) subtraction spectrum (Fig. 11d) signalled the presence of a genuine OH-bond vibrational band formed due to the water steam treatment of the mixed TiP and APTES precursors. The establishment of the H bonding network was important because it enabled the bonding

of the sol–gel hybrid to the bound water molecules present in the non-crystalline region of cellulose (Hofstetter et al. 2006).

Finally, the ATR evidence of the protonation of the amino groups was sought because this protonation is responsible for the bactericidal properties. From the spectra shown in Figs. 11 and 12, in the transmission (Fig. 12b) and ATR (Fig. 11b) spectra of APTES, the NH_2 deformational band was found at 1597 cm^{-1}, while in the spectra of TiP/APTES, the band became broader and split into two bands in the 1550–1505 cm^{-1} spectral region (Figs. 11c, 12c), signalling the protonation of the amide groups (Bellamy 1954). The protonation of the APTES in the latter spectra could be explained by the presence of a more acidic TiP precursor. The protonation of APTES could be easily achieved, even when the APTES was deposited on a titanium metal surface (isoelectric point 6.0), while no protonated amine was observed when the APTES was deposited on a Ni metal surface (isoelectric point 10–12) (Horner et al. 1992). In summary, in the TiP/APTES hybrid, the TiP played the role of a hydroxylated acidic surface, which was necessary for realizing protonated APTES and imparting bactericidal properties to the hybrid nanocomposite.

ATR IR spectra of the cotton samples

ATR spectra of cotton: background selection We began investigations of the cotton finishes by measuring the ATR spectra of untreated cotton fabrics (cotton as-received) and fabrics stored overnight in an EtOH water solution, dipped in boiling water, and then dried (EtOH/cotton) (see "Experimental" section) (Fig. 13A, B). The latter spectra were required to obtain the subtraction spectra, which enable the characterization of the sol–gel hybrids on the cotton fabrics. The spectra were baseline corrected to 0 in the 4000–400 cm^{-1} region and normalized to 1 at 1160 cm^{-1}, the absorbance peak reflecting the carbohydrate backbone. The ATR spectra of both cotton samples showed typical bands attributed to the OH stretching mode of cellulose at 3412 cm^{-1} (O_2H–O_6, intra), 3326 cm^{-1} (O_3H–O_5, intra) and 3266 cm^{-1} (O_6H–O_3, intermolecular H bond) (Tsuboi 1957; Maréchal and Chanzy 2000; Chung et al. 2004; Hinterstoisser et al. 2001; Hinterstoisser and Salmén 1999).

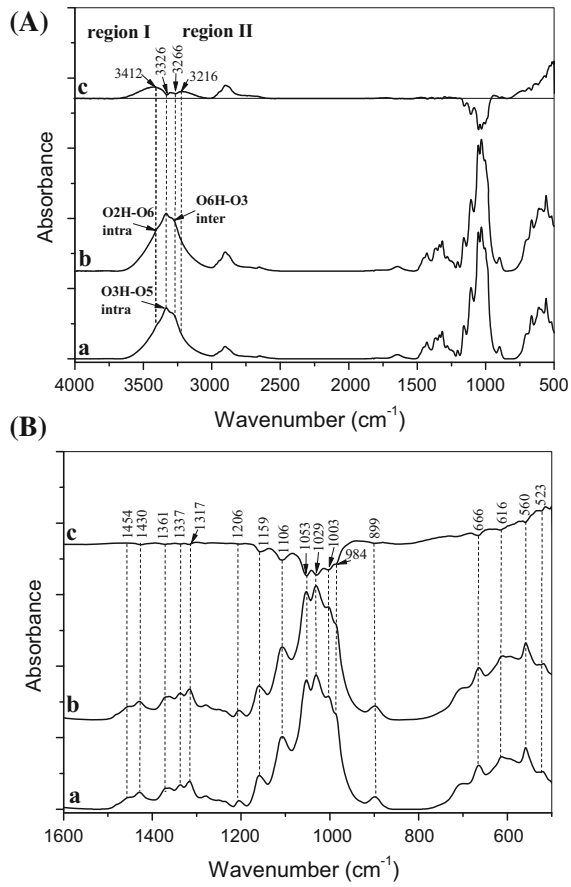

Fig. 13 ATR spectra of cotton as-received (*a*), cotton treated in EtOH and the boiling water (EtOH/cotton) (*b*) and the subtraction spectrum of (EtOH/cotton—cotton as-received) (*c*) in the spectral region from 4000 to 500 cm^{-1} (**A**) and in the spectral region from 1600 to 500 cm^{-1} (**B**)

The corresponding subtraction spectrum (EtOH/cotton—cotton as-received) (c in Fig. 13A) revealed that the OH–O band (3500–2700 cm^{-1}) gained intensity in the high (>3400 cm^{-1}, region I) and low (~3200 cm^{-1}, region II) frequency wings (as denoted in Fig. 13A) of the OH–O band. We attributed the intensity increase in region I to the presence of loosely bound water molecules ("free" water absorbs <3500 cm^{-1}), i.e., water indirectly bonded to the OH groups via another water molecule, while the presence of the 3200 cm^{-1} band (region II) was associated with strongly bound water (Walrafen and Klein 1987), i.e., water bound directly by hydrogen bonds to the OH groups of the cellulose (Olsson and Salmén 2004). Treatment of the cotton substrates with EtOH followed by dipping in boiling water strongly affected the

proportion of water that was more loosely versus strongly bonded to the cellulose. Changes were also observed in the fingerprint spectral region (1160–900 cm^{-1}), where the ring skeletal modes appear as negative bands, indicating that they were partially lost during the EtOH/boiling water treatment (Fig. 13B) (Maréchal and Chanzy 2000). However, all of the bands were negative, and they did not show frequency shifts or band shape changes. In contrast, Hinterstoisser and Salmen (1999) observed a small (few cm^{-1}) shift in the frequency of the 1,2-glucosid (–C–O–C–) band at 1158 cm^{-1} in the spectra of cellulose exposed to different humidity conditions. The most important observation was that the water uptake during the EtOH/boiling water treatment affected cotton selectively; more water was adsorbed on the easily accessible water sites (region I) than on sites with strongly absorbed water molecules (region II). This finding is not new and is in agreement with the moisture uptake study using dynamic IR and deuterium exchange performed by Hofstetter et al. (2006). Accordingly, to obtain the subtraction spectra, only the EtOH/cotton spectrum was used as the background.

ATR spectra of the coated cotton samples The ATR spectra of the TiP-coated cotton (TiP/cotton) and TiP/APTES-coated cotton (TiP/APTES/cotton) samples (Fig. 14) were examined to confirm the presence of hybrids on the cotton fabrics and, by inspecting the characteristic bands in the corresponding subtraction spectra (Fig. 15), to ascertain their interactions with the cotton fibres. The main challenge was to show the existence of the Si–O–C bonds known to form between the silanes and the OH groups of cellulose at elevated temperatures (Xie et al. 2010). To identify the corresponding modes in the ATR spectra, the TiP/cotton and TiP/APTES/cotton samples were exposed to heat treatment at 105 °C (24 h), and the corresponding subtraction spectra were examined (Fig. 16).

The ATR spectra of the TiP/cotton and TiP/APTES/cotton samples (Fig. 14) were very similar because the massive absorption of the cellulose bands blurred the vibrational bands of the applied finishes. This was not surprising as the amount of hybrids on the cotton was only a few percent. Nonetheless, the subtraction procedure gave reproducible spectra with good signals, as has been demonstrated in our previous

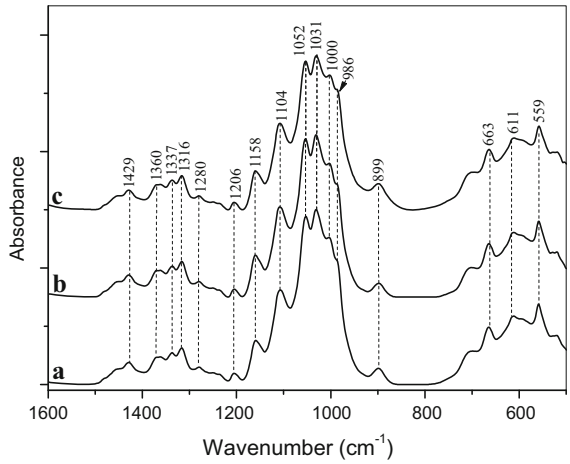

Fig. 14 ATR spectra of cotton as-received (*a*), TiP/cotton (*b*) and TiP/APTES/cotton (*c*) in the spectral region from 1600 to 500 cm^{-1}

studies of other finished cotton samples (Vilčnik et al. 2009; Vince et al. 2006).

A closer look at the subtraction spectra of (TiP/cotton—EtOH/cotton), (TiP/APTES/cotton—EtOH/cotton) and (TiP/APTES/cotton—TiP/cotton) samples (a, b and c in Fig. 15A) revealed expected changes in the spectral region from 3700 to 2700 cm^{-1}, where the OH stretching bands appeared. The broad OH···O stretching band was split into high (region I) and low frequency wings (region II), similar to the (EtOH/cotton—cotton as-received) subtraction spectrum (c in Fig. 13A). However, the intensity of the OH stretching band in region II was greater than that in region I, which suggested preferential occupation (bonding) of the TiP/APTES hybrid on the strongly bonded water molecules of cellulose or, even more likely, the presence and bonding of the hybrids on the fibres. The redshifted band maxima of the positive OH stretching band in the subtraction spectra (Fig. 15A) at 3030 cm^{-1} (a in Fig. 15A), 3060 cm^{-1} (b in Fig. 15A), and 3106 cm^{-1} (c in Fig. 15A) suggested that the strongest H-bonding occurred in the TiP/cotton finishes. In conclusion, at ambient temperatures, the hybrids bonded preferentially to the strongly bonded water molecules of cellulose (Hinterstoisser and Salmén 1999).

The subtraction spectra (Fig. 15B) in the 1700–500 cm^{-1} spectral region did not confirm directly the existence of TiP hybrid on fibres because TiP did not show distinct band in this spectral region as

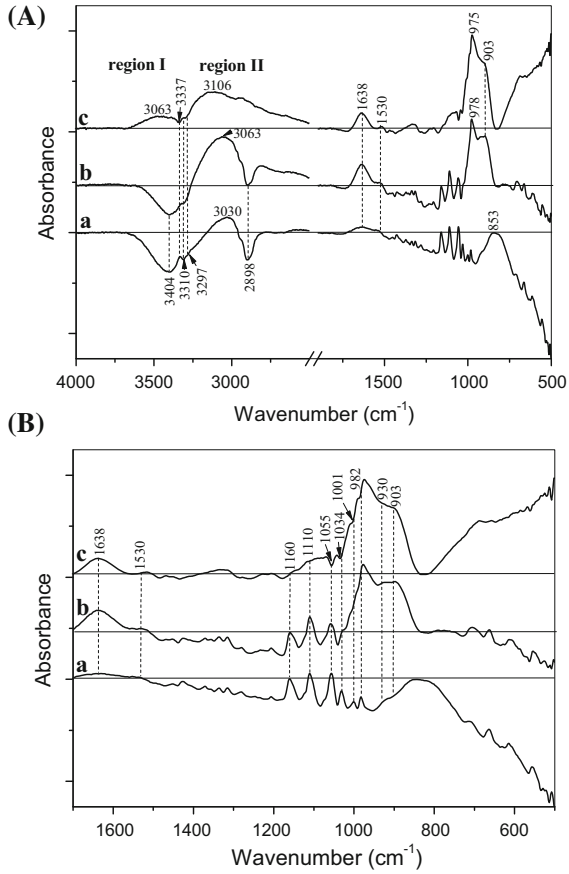

Fig. 15 Subtraction spectra of TiP/cotton—EtOH/cotton (*a*), TiP/APTES/cotton—EtOH/cotton (*b*) and TiP/APTES/cotton—TiP/cotton (*c*) samples in the spectral region from 4000 to 500 cm^{-1} (**A**) and in the spectral region from 1700 to 500 cm^{-1} (**B**)

silica. However, in the TiP/APTES spectrum, i.e., the (TiP/APTES/cotton—EtOH/cotton) subtraction spectrum (b in Fig. 15B), we observed strong positive bands at 978 and 903 cm^{-1}, which can be attributed to the Si–O–Si and Si–O–Ti modes. The latter mode corresponded nearly exactly to the Si–O–Ti band observed in the ATR spectra of the corresponding hybrid coatings prepared in the absence of cotton (c in Fig. 11). The redshift in the frequency of the Si–O–Si band ($\Delta\nu \sim -20$ cm^{-1}) suggested that the structure of the hybrid network was modified in the presence of cellulose, while the strong Si–O–Ti band, which indicated high extent of crosslinking between both precursors and their intimate mixing, did not change

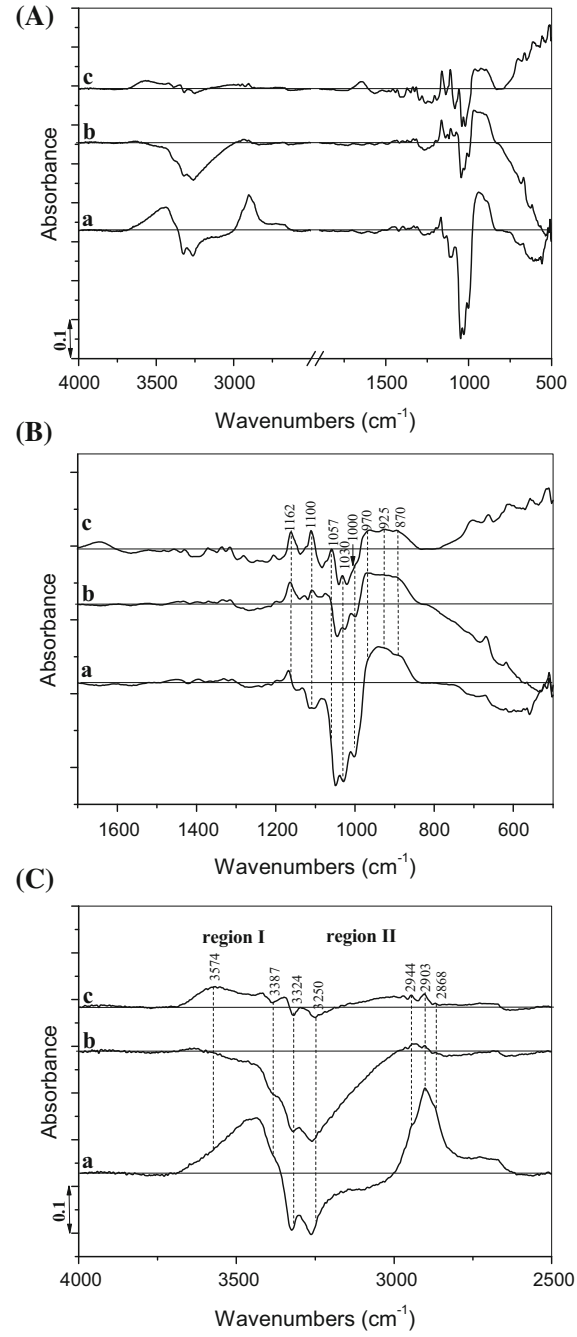

Fig. 16 Subtraction spectra of TiP/APTES/cotton (105 °C)—cotton-as received (*a*), TiP/APTES/cotton—EtOH/cotton (*b*) and TiP/APTES/cotton (105 °C)—cotton-as received (105 °C) (*c*) samples in the spectral region from 4000 to 500 cm^{-1} (**A**), in the spectral region from 1700 to 500 cm^{-1} (**B**) and in the spectral region from 4000 to 2500 cm^{-1} (**C**)

markedly. We attributed these results to the synthesis route; non-hydrolysed TiP and APTES precursors penetrated the fibres, where they were simultaneously subjected to hydrolysis in the boiling water for a very short time, which prevented the formation of separate silica and titania networks and the formation of nanoparticles (Schraml-Marth et al. 1992).

It is important to note that the skeletal modes of the cellulose (1158, 1104, 1052, 1031, 1000 and 986 cm^{-1}) (Fig. 14) changed slightly, indicating that they were not strongly affected by the application of the TiP/APTES and TiP hybrids. The interactions were rather weak, as suggested by the small frequency shifts in the cellulose skeletal bands at 1160, 1110, 1055, 1001 and 978 cm^{-1} in the (TiP/APTES/cotton—TiP/cotton) subtraction spectrum (b in Fig. 15B). But the bands at 1000 and 986 cm^{-1} diminished in intensity and became weaker compared to the other skeletal bands (1160, 1110, 1055 cm^{-1}), which suggested that they were preferentially consumed due to interactions with the Ti–OH groups in the TiP hybrid.

It should also be mentioned that the (TiP/APTES/cotton—EtOH/cotton) subtraction spectrum (b in Fig. 15B) confirmed that the protonation of the TiP/APTES reached completion. A strong band was observed at 1530 cm^{-1} (NH_3^+) in these spectrum, in contrast to the (TiP/cotton—EtOH/cotton) subtraction spectrum (a in Fig. 15B).

Although the positive bands at 978, 930 and 903 cm^{-1} (b in Fig. 15B) confirmed the presence of the TiP/APTES hybrid on cotton, they did not provide direct proof of the establishment of the Si–O–C bonds conceived from the XPS studies (Figs. 3, 4) that were expected to form due to the condensation reactions between the sol–gel hybrids and the OH groups of the cellulose. The formation of covalent Si–O–C bonds was proposed and anticipated by different authors (Xie et al. 2010; Abdelmouleh et al. 2002; Mihailović et al. 2011; Valadez-Gonzalez et al. 1999), but the OH groups of the cellulose, which may be involved in the formation of the covalent Si–O–Si bonds, have not yet been clearly identified from the ATR spectra. Because it has already been determined that, for heat treated cotton finishes, refluxing the fibres does not remove the finishes, we exposed the TiP/APTES/cotton, TiP/cotton and EtOH/cotton samples to heat treatment (105 °C, 24 h). The subtraction spectra of the [(TiP/APTES/cotton (105 °C)—cotton as-received), a in Fig. 16], [(TiP/APTES/cotton (105 °C)—EtOH/cotton), b in Fig. 16] and [(TiP/APTES/cotton (105 °C)—EtOH/cotton (105 °C), c in Fig. 16] samples were constructed and compared to the subtraction spectra of the non-heated cotton finishes (a, b in Fig. 14).

The corresponding subtraction spectra (Fig. 16) showed that the –C–OH bands, which were attributed to the primary and secondary alcohol groups of cellulose (Maréchal and Chanzy 2000; Hinterstoisser and Salmén 1999) at 1057, 1030 and 1000 cm^{-1} (c in Fig. 16B), were negative, which indicated that the primary and secondary alcohol groups (C–OH) were consumed when the TiP/APTES hybrid was applied to the cotton fabrics and then heated at 105 °C. Other skeletal bands at 1162, 1100 and 1057 cm^{-1} had slightly shifted frequencies, which indicated that they were also affected by the interactions with the silanol groups. However, more apparent was the negative absorption in the frequency window from 1150 to 1000 cm^{-1}, which was not observed in the subtraction spectra of the as-prepared, i.e., non-heated, TiP/APTES spectrum (b in Fig. 15B). The Si–O–Si and Si–O–Ti bands (970, 925 and 870 cm^{-1}) were clearly observed in both subtraction spectra.

The most intense negative bands were found in the (TiP/APTES/cotton—cotton as-received) subtraction spectrum (a in Fig. 16B), while the negative bands observed in the spectrum obtained by the subtraction of EtOH/cotton (b in Fig. 16B) and cotton as-received and heat treated at 105 °C (c in Fig. 16B) were less pronounced. It should be noted that the observed negative bands in the spectral region of the skeletal bands of cotton (1150–1000 cm^{-1}, Fig. 16B) were also reported by Valadez-Gonzales et al. (1999), but the authors did not attribute the corresponding negative absorption to the elimination of the skeletal bands in the cellulose [henéquen (*Agave fourcroydes*)] and thus to the interaction sites between the silane molecules and the cellulose. It seems that henéquen fibres are more susceptible to interactions with silanes, which we could attribute to the presence of lignin, which is known to interact strongly with silanes (Rasmussen et al. 2014b). Our cotton did not contain lignin.

The heat-treatment of the fabrics also changed the water content, as shown by the corresponding O–H···O bands (Fig. 16C). The subtraction of the as-received cotton heat treated at 105 °C from the TiP/

APTES/cotton heat treated at 105 °C showed relatively weak negative O–H bands in the spectral region 3600–2800 cm^{-1} corresponding to the O_6H–O_3 vibrational band at ~3250 cm^{-1}, the O_5H–O_2 intramolecular mode at ~3324 cm^{-1} and the O_6H–O_2 band at ~3387 cm^{-1} (c in Fig. 16C). This result indicated that the heat-treatment of the fabrics changed their water contents and suggested that some of the −OH groups were consumed by the silanol groups due to the condensation reactions. The condensation was not complete, as could be inferred from the presence of a positive band at 3574 cm^{-1}. This band indicated that some of the O–H groups were free of hydrogen bonding. We tentatively assigned the corresponding band to the "free" Si–OH groups of the TiP/APTES hybrids, although the assignment of this band to the C–OH stretching mode is also possible (Maréchal and Chanzy 2000).

Expectedly, the genuine intra and inter O–H···O bands of cotton were more intense and negative in the spectra obtained by the subtraction of the as-received cotton and the EtOH/cotton spectra from the TiP/APTES/cotton spectrum (105 °C) (b and c in Fig. 16C), indicating that more water (loosely and strongly bonded) existed in the corresponding cotton samples than in the heated samples. However, the positive band in region I (a in Fig. 16C) suggested that the TiP/APTES after the heat treatment preferentially bonded to the water molecules indirectly linked to the OH groups via another water molecule (Walrafen and Klein 1987) and not to the water bound directly by hydrogen bonds to the OH groups of the cellulose (Olsson and Salmén 2004), as occurred at ambient temperature (b in Fig. 15). This finding was consistent with the penetration of the TiP/APTES within the cotton fabrics and its bonding to the cellulose. Obviously, the interactions were not limited to the water system of cellulose; they also affected other molecular sites in cellulose, as shown by the characteristic bands at 1057, 1030 and 1000 cm^{-1} and described above (Fig. 16B).

TG measurements

TG analysis enables the estimation of the amount of the hybrid attached to the cotton fibre surface and can provide complementary information about the thermal behaviours of the hybrid coatings deduced from either elemental analysis or infrared spectroscopy. The TG analyses (Fig. 17) of the cotton fibres revealed that the pyrolysis of the cotton fibres included three stages: initial, main, and char decomposition (Zhu et al. 2004). In the initial stage below 300 °C, the weight loss is small and attributed to the loss of water. In the temperature range of 300–380 °C, the main pyrolysis stage occurs, and the weight loss was quite significant. It is known that the first stage involves changes in the amorphous part of the cellulose, while in the second stage, pyrolysis occurs in the crystalline regions of the cellulose fibres (Zhu et al. 2004). In the third stage, char is produced (T > 430 °C), and water and carbon dioxide form.

The results of the TG measurements of the TiP/APTES/cotton and TiP/cotton samples revealed that the mass losses of the cotton and finished cotton fibres were as expected. It should be noted that the mass that remained after heating the untreated cotton (i.e.,

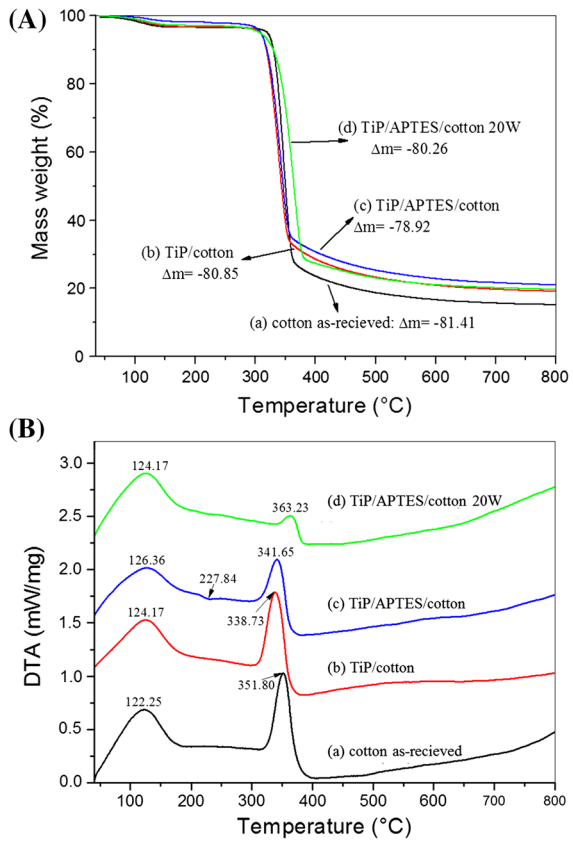

Fig. 17 TG (**A**) and DTA (**B**) graphs for cotton as-received (*a*), TiP/cotton (*b*) and TiP/APTES/cotton (*c*) and TiP/APTES/cotton after twenty consecutive washing (20 W) (*d*) samples analysed in a nitrogen atmosphere

18.59 %) in N_2 was a few percent higher than the mass losses obtained after heating the untreated cotton in air (Vasiljević et al. 2015; Xue et al. 2009). To avoid errors due to the complex pyrolysis mechanism, the measurements were repeated several times with increasing initial masses of the finished samples (up to 100 mg), i.e., up to 5–10 times. The as-received cotton sample (Fig. 17) showed a mass loss $\Delta m = -81.41$ %, exceeding the mass losses observed for the TiP/cotton ($\Delta m = -80.85$ %) and the TiP/APTES/cotton ($\Delta m = -78.92$ %) samples. The small mass losses were not surprising due to the short dipping times of the cotton fibres in the boiling water. Similarly, the shift in the maximal temperature of the mass change obtained from the dTG measurements was only few degrees (not shown here). The washed TiP/APTES/cotton sample had slightly higher mass losses than the untreated cotton ($\Delta m = -80.26$ %). In addition, TiP/APTES/cotton sample showed DTA curve which differed compared to the DTA curves of bare cotton and TiP/cotton samples. The heat changes in the temperature interval from 220 to 250 °C were attributed to the condensation reactions of the TiP/APTES hybrid competing with the loss of the amino groups of the APTES part of the hybrid. Unfortunately, we were not able to obtain Δm for the TiP/cotton sample; repetitive measurements gave scattered results ($\Delta m = \pm 0.5$ %), which indicated that the TiP coating was too small to provide reliable mass losses.

Conclusions

The soaking of cotton fabric in non-hydrolysed solutions of precursors followed by quick immersion in boiling water was an efficient method for the impregnation of cotton fabric with TiP/APTES, and to a lesser extent, with TiP hybrids, as shown in the SEM and EDX micrographs. Due to the short immersion time in the boiling water, the TiP/APTES hybrids were amorphous and resembled amino-functionalized polymers. The TiP hybrids were in the form of nanoparticles with sizes of 5–10 nm, as observed in the TEM images. These morphological differences caused differences in the photocatalytic activity; while TiP/APTES did not have any photocatalytic activity, TiP degraded BPB quite effectively. An additional advantage of low-temperature fibre processing, was the impregnation of the cotton fibres throughout their volume, contrasting surface coating depositions when other methods are applied. Infrared ATR measurements of the cotton hybrids revealed that the anchoring of the TiP/APTES hybrids at ambient temperatures occurred via the water bound directly by hydrogen bonds to the OH groups of the cellulose. Loosely bonded water also participated in bonding the hybrids to cellulose, but to a lesser extent. No covalent bonding of the hybrids to the OH groups of cellulose could be inferred from the ATR spectra; however, Si–O–C bonding was confirmed for the cotton heat treated at 105 °C.

The lack of covalent Si–O–C bonding was not detrimental to obtaining stable UPF and bacteriostatic properties because the interpenetrating H-bonding systems of cellulose and the hybrids as well as the presence of the hybrids inside the fabric provided sufficient mobility of the hybrid molecules or fragments and their expulsion to the fabric surface when the cotton fabrics were repetitively washed. This behaviour explained the stability of the bacteriostatic photocatalytic efficiency of the TiP/APTES hybrids, which dropped by ~ 10 %, and the variation in the UPF and bacteriostatic effects with washing and UV illumination observed for the TiP-coated cotton. We primarily ascribed the enhanced bacteriostatic effect of the TiP/APTES relative to the TiP-coated cotton samples to the presence of protonated amino groups. Further work is planned to apply the cotton finishes using heat treatment.

Acknowledgments Authors dedicate this article to doc. Dr. Vojmir Francetič who sadly passed away during the preparation of this work. This work was supported by the Slovenian Research Agency (Programmes P2-0213 and P2-0393). The authors would like to thank dr. Urban Novak from the National Institute of Chemistry for performing the IR spectroscopic measurements.

References

Abdelmouleh M, Boufi S, ben Salah A, Belgacem MN, Gandini A (2002) Interaction of silane coupling agents with cellulose. Langmuir 18:3203–3208

Aizawa M, Nosaka Y, Fujii N (1991) FT-IR Liquid attenuated total reflection study of TiO_2–SiO_2 sol–gel reaction. J Non-Cryst Solids 128:77–85

Angeloni L, Marzocch MP, Hadzi D, Orel B, Sbrana G (1974) Symmetric hydrogen bonding—infrared-absorption spectrum of potassium hydrogen succinate single-crystal. Chem Phys Lett 28:201–204

Arkles BC, Larson GL (2004) Silicon compounds: silanes and silicones: a survey of properties and chemistry. Gelest Inc, Morrisville

Avbelj F, Orel B, Klanjsek M, Hadzi D (1985) Vibrational-spectra of potassium hydrogen maleate crystal and solution. Spectrochim Acta A 41:75–87

Bacsa RR, Grätzel M (1996) Rutile formation in hydrothermally crystallized nanosized titania. J Am Ceram Soc 79:2185–2188

Belgacem MN, Czeremuszkin G, Sapieha S, Gandini A (1995) Surface characterization of cellulose fibres by XPS and inverse gas chromatography. Cellulose 2:145–157

Bellamy LJ (1954) The infra-red spectra of complex molecules. Methuen, London **(New York: Wiley)**

Brinker CJ, Scherer GW (1990) Sol–gel science: the physics and chemistry of sol–gel processing. Academic Press, Boston

Brooks RE, Moore SB (2000) Alkaline hydrogen peroxide bleaching of cellulose. Cellulose 7:263–286

Castellano M, Gandini A, Fabbri P, Belgacem MN (2004) Modification of cellulose fibres with organosilanes: Under what conditions does coupling occur? J Colloid Interface Sci 273:505–511

Čepin M, Jovanovski V, Podlogar M, Crnjak Orel Z (2015) Amino- and ionic liquid-functionalised nanocrystalline ZnO via silane anchoring—an antimicrobial synergy. J Mater Chem B 3:1059–1067

Chemseddine A, Moritz T (1999) Nanostructuring titania: Control over nanocrystal structure, size, shape, and organization. Eur J Inorg Chem 2:235–245

Chung C, Lee M, Choe EK (2004) Characterization of cotton fabric scouring by FT-IR ATR spectroscopy. Carbohydr Polym 58:417–420

Colleoni C, Massafra MR, Rosace G (2012) Photocatalytic properties and optical characterization of cotton fabric coated via sol–gel with non-crystalline TiO_2 modified with poly(ethylene glycol). Surf Coat Technol 2017:79–88

Čolović M, Jerman I, Gaberšček M, Orel B (2011) POSS based ionic liquid as an electrolyte for hybrid electrochromic devices. Sol Energy Mater Sol C 95:3472–3481

Daniels MW, Francis LF (1998) Silane adsorption behavior, microstructure, and properties of glycidoxypropyltrimethoxysilane-modified colloidal silica coatings. J Colloid Interface Sci 205:191–200

Daoud WA, Xin JH, Zhang YH (2005) Surface functionalization of cellulose fibers with titanium dioxide nanoparticles and their combined bactericidal activities. Surf Sci 599:69–75

Duan J, Kasper DL (2011) Oxidative depolymerization of polysaccharides by reactive oxygen/nitrogen species. Glycobiology 21:401–409

Fir M, Orel B, Vuk AS, Vilčnik A, Ješe R, Francetič V (2007) Corrosion studies and interfacial bonding of urea/poly(dimethylsiloxane) sol/gel hydrophobic coatings on AA 2024 aluminum alloy. Langmuir 23:5505–5514

Fujishima A, Hashimoto K, Watanabe T (1999) TiO_2 photocatalysis—fundamentals and applications. BKC Inc, Tokyo

Fukatsu K, Kokot S, Schweinsberg DP (1999) Bleaching of cotton fabric with electrogenerated oxygen—the role of hydroxyl and superoxide radicals. Text Res J 69:769–775

Galkina OL, Sycheva A, Blagodatskiy A, Kaptay G, Katanaev VL, Seisenbaeva GA, Kessler VG, Agafonov AV (2014) The sol–gel synthesis of cotton/TiO_2 composites and their antibacterial properties. Surf Coat Technol 253:171–179

Hadzi D, Orel B (1973) OH-stretching band of acid salts of carboxylic-acids and symmetry of hydrogen-bond. J Mol Struct 18:227–239

Hinterstoisser B, Salmén L (1999) Two-dimensional step-scan FT-IR: a tool to unravel the OH-valency-range of the spectrum of Cellulose I. Cellulose 6:251–263

Hinterstoisser B, Akerholm M, Salmén L (2001) Effect of fiber orientation in dynamic FT-IR study on native cellulose. Carbohydr Res 334:27–37

Hofstetter K, Hinterstoisser B, Salmén L (2006) Moisture uptake in native cellulose—the roles of different hydrogen bonds: a dynamic FT-IR study using Deuterium exchange. Cellulose 13:131–145

Horner MR, Boerio FJ, Clearfield HM (1992) An XPS investigation of the adsorption of aminosilanes onto metal substrates. J Adhes Sci Technol 6:1–22

Hu C, Guo J, Qu J, Hu X (2007) Photocatalytic degradation of pathogenic bacteria with AgI/TiO_2 under visible light irradiation. Langmuir 23:4982–4987

Ibáñez JA, Litter MI, Pizarro RA (2003) Photocatalytic bactericidal effect of TiO_2 on *Enterobacter cloacae*: comparative study with other Gram (−) bacteria. J Photochem Photobiol, A 15:81–85

Isquith AJ, Abbott EA, Walters PA (1972) Surface-bonded antimicrobial activity of an organosilicon quaternary ammonium chloride. Appl Microbiol 24:859–863

Jerman I, Vuk AU, Kozelj M, Orel B, Kovac J (2008) A structural and corrosion study of triethoxysilyl functionalized POSS coatings on AA 2024 alloy. Langmuir 24:5029–5037

Jerman I, Mihelčič M, Koželj M, Orel B (2012) Sol–gel based spectrally selective solar absorber coatings and the process for producing said coatings. WO 2013/158049

Kikuchi Y, Sunada K, Iyoda T, Hashimoto K, Fujishima A (1997) Photocatalytic bactericidal effect of TiO_2 thin films: dynamic view of the active oxygen species responsible for the effect. J Photochem Photobiol, A 106:51–56

Kiwi J, Nadtochenko V (2005) Evidence for the mechanism of photocatalytic degradation of the bacterial wall membrane at the TiO_2 interface by ATR-FTIR and laser kinetic spectroscopy. Langmuir 21:4631–4641

Kotani Y, Matsuda A, Tatsumisago M, Minami T, Umezawa T, Kogure T (2000) Formation of anatase nanocrystals in sol–gel derived TiO_2–SiO_2 thin films with hot water treatment. J Sol-Gel Sci Technol 19:585–588

Kowal K, Cronin P, Dworniczek E, Zeglinski J, Tiernan P, Wawrzynska M, Podbielska H, Tofail SAM (2014) Biocidal effect and durability of nano-TiO_2 coated textiles to combat hospital acquired infections. RSC Adv 4:19945–19952

Koželj M, Vuk AS, Jerman I, Orel B (2009) Corrosion protection of Sunselect, a spectrally selective solar absorber coating, by (3-mercaptopropyl)trimethoxysilane. Sol Energy Mater Sol C 93:1733–1742

Ku H, Wang H, Pattarachaiyakoop N, Trada M (2011) A review on the tensile properties of natural fiber reinforced polymer composites. Compos Part B Eng 4:856–873

Kumar K-NP, Kumar J, Keizer K (1994) Effect of Peptization on densification and phase-transformation behavior of sol–

gel-derived nanostructured titania. J Am Ceram Soc 77:1396–1400

Kumar A, Pandey AK, Singh SS, Shanker R, Dhawan A (2011) Engineered ZnO and TiO_2 nanoparticles induce oxidative stress and DNA damage leading to reduced viability of *Escherichia coli*. Free Radical Biol Med 51:1872–1881

Langlet M, Kim A, Audier M, Herrmann JM (2002) Sol–gel preparation of photocatalytic TiO_2 films on polymer substrates. J Sol-Gel Sci Technol 25:223–234

Langlet M, Kim A, Audier M, Guillard C, Herrmann JM (2003) Liquid phase processing and thin film deposition of titania nanocrystallites for photocatalytic applications on thermally sensitive substrates. J Mater Sci 38:3945–3953

Li Z, Hou B, Xu Y, Wu D, Sun Y (2005) Hydrothermal synthesis, characterization, and photocatalytic performance of silica-modified titanium dioxide nanoparticles. J Colloid Interface Sci 288:149–154

Li Q, Mahendra S, Lyon DY, Brunet L, Liga MV, Li D, Alvarez PJJ (2008) Antimicrobial nanomaterials for water disinfection and microbial control: potential applications and implications. Water Res 42:4591–4602

Linsebigler AL, Lu G, Zates JT (1995) Photocatalysis on TiO_2 surfaces—principles, mechanisms, and selected results. Chem Rev 95:745–758

Liu P, Duan W, Wang Q, Li X (2010) The damage of outer membrane of *Escherichia coli* in the presence of TiO_2 combined with UV light. Colloid Surface B 78:171–176

Lu Z-X, Zhou L, Zhang Z-L, Shi W-L, Xie Z-X, Xie H-Y, Pang D-W, Shen P (2003) Cell damage induced by photocatalysis of TiO_2 thin films. Langmuir 19:8765–8768

Mahltig B, Böttcher H, Rauch K, Dieckmann U, Nitsche R, Fritz T (2005) Optimized UV protective coatings by combination of organic and inorganic UV absorbers. Thin Solid Films 485:108–114

Mahltig B, Gutmann E, Meyer DC, Reibold M, Dresler B, Günther K, Faßler D, Böttcher H (2007) Solvothermal preparation of metallized titania sols for photocatalytic and antimicrobial coating. J Mater Chem 17:2367–2374

Malešič J, Kolar J, Strlič M, Kočar D, Fromageot D, Leamaire J, Haillant O (2005) Photo-induced degradation of cellulose. Polym Degrad Stab 89:64–69

Maness PC, Smolinski S, Blake DM, Huang Z, Wolfrum EJ, Jacoby WA (1999) Bactericidal activity of photocatalytic TiO_2 reaction: toward an understanding of its killing mechanism. Appl Environ Microbiol 65:4094–4098

Maréchal Y, Chanzy H (2000) The hydrogen bond network in Iβ cellulose as observed by infrared spectrometry. J Mol Struct 523:183–196

Matsuda A, Kotani Y, Kogure T, Tatsumisago M, Minami T (2000) Transparent anatase nanocomposite films by the sol–gel process at low temperatures. J Am Ceram Soc 83:229–231

Matsuda A, Matoda T, Kotani Y, Kogure T, Tatsumisago M, Minami T (2003) Evaluation of photocatalytic activity of transparent anatase nanocrystals-dispersed silica films prepared by the sol–gel process with hot water treatment. J Sol-Gel Sci Technol 26:517–521

Matsunaga T, Tomoda R, Nakajima T, Nakamura N, Komine T (1988) Continuous-sterilization system that uses photosemiconductor powders. Appl Environ Microbiol 54:1330–1333

Mihailović D, Šaponjić Z, Radoičić M, Lazović S, Baily CJ, Jovančić P, Nedeljković J, Radetić M (2011) Functionalization of cotton fabrics with corona/air RF plasma and colloidal TiO_2 nanoparticles. Cellulose 18:811–825

Mihelčič M, Francetič V, Pori P, Gradišar H, Kovač J, Orel B (2014) Electrochromic coatings made of surface modified rutile and anatase pigments: influence of trisilanol POSS dispersant on electrochromic effect. Appl Surf Sci 313:484–497

Milović NM, Wang J, Lewis K, Klibanov AM (2005) Immobilized N-alkylated polyethylenimine avidly kills bacteria by rupturing cell membranes with no resistance developed. Biotechnol Bioeng 90:715–722

Moulder JF, Stickle WF, Sobol PE, Bomben KD (1995) Handbook of X-ray photoelectron spectroscopy. Physical Electronics Inc., Eden Prairie

Nadtochenko VA, Sarkisov OM, Nikandrov VV, Chubukov PA, Denisov NN (2008) Inactivation of pathogenic microorganisms in the photocatalytic process on nanosized TiO_2 crystals. Russ J Phys Chem B 2:105–114

Nur H (2006) Modification of titanium surface species of titania by attachment of silica nanoparticles. Mater Sci Eng B Solid 133:49–54

Olsson AM, Salmén L (2004) The association of water to cellulose and hemicellulose in paper examined by FTIR spectroscopy. Carbohydr Res 339:813–818

Orel B, Ješe R, Stangar UL, Grdadolnik J, Puchberger M (2005a) Infrared attenuated total reflection spectroscopy studies of aprotic condensation of (EtO)(3)Si-R-Si(OEt)(3) and R-Si(OEt)(3) systems with carboxylic acids. J Non-Cryst Solids 351:530–549

Orel B, Ješe R, Vilčnik A, Stangar UL (2005b) Hydrolysis and solvolysis of methyltriethoxysilane catalyzed with HCl or trifluoroacetic acid: IR spectroscopic and surface energy studies. J Sol-Gel Sci Technol 34:251–265

Panarin EF, Solovskii MV, Ékzemplyarov ON (1971) Synthesis and antimicrobial properties of polymers containing quaternary ammonium groups. Pharm Chem J 5:406–408

Puzenat E, Pichat P (2003) Studying TiO_2 coatings on silica-covered glass by O_2 photosorption measurements and FTIR–ATR spectrometry: correlation with the self-cleaning efficacy. J Photochem Photobiol, A 160:127–133

Qi K, Daud WA, Xin JH, Mak CL, Tang W, Cheung WP (2006) Self-cleaning cotton. J Mater Chem 16:4567–4576

Radetić M (2013) Functionalization of textile materials with TiO_2 nanoparticles. J Photochem Photobiol, C 16:62–76

Rasmussen JS, Barsberg S, Felby C (2014a) Complex between lignin and a Ti-based coupling agent. Holzforschung 68:541–548

Rasmussen JS, Barsberg S, Venas TM, Felby C (2014b) Assessment of covalent bond formation between coupling agents and wood by FTIR spectroscopy and pull strength tests. Holzforschung 68:799–805

Saito T, Iwase T, Horie J, Morioka T (1992) Mode of photocatalytic bactericidal action of powdered semiconductor TiO_2 on mutans streptococci. J Photochem Photobiol, B 14:369–379

Saravanan D (2007) UV protection textile materials. AUTEX Res J 7:53–62

Schraml-Marth M, Walther KL, Wokaun A, Handy BE, Baiker A (1992) Porous silica gels and TiO_2/SiO_2 mixed oxides

prepared via the sol-gel process: characterization by spectroscopic techniques. J Non-Cryst Solids 143:93–111

Simončič B, Tomšič B, Černe L, Orel B, Jerman I, Kovač J, Žerjav M, Simončič A (2012) Multifunctional water and oil repellent ant antimicrobial properties of finished cotton: influence of sol–gel finishing procedure. J Sol-Gel Sci Technol 61:340–354

Simončič B, Hadžić S, Vasiljević J, Černe L, Tomšič B, Jerman I, Orel B, Medved J (2014) Tailoring of multifunctional cellulose fibres with "lotus effect" and flame retardant properties. Cellulose 21:595–605

Subramanian E, Subbulakshmi S, Murugan C (2014) Inter-relationship between nanostructures of conducting polyaniline and the photocatalytic methylene blue degradation efficiencies of its hybrid composites with anatase TiO_2. Mater Res Bull 51:128–135

Sunada K, Kikuchi Y, Hashimoto K, Fujishima A (1998) Bactericidal and detoxification effects of TiO_2 thin film photocatalysts. Environ Sci Technol 32:726–728

Sunada K, Watanabe T, Hashimoto K (2003) Studies on photokilling of bacteria on TiO_2 thin film. J Photochem Photobiol, A 156:227–233

Thevenot P, Cho J, Wavhal D, Timmons RB, Tang L (2008) Surface chemistry influences cancer killing effect of TiO_2 nanoparticles. Nanomed Nanotechnol 4:226–236

Timofeeva L, Kleshcheva N (2011) Antimicrobial polymers: mechanism of action, factors of activity, and applications. Appl Microbiol Biotechnol 89:475–492

Tomšič B, Klemenčič D, Simončič B, Orel B (2011) Influence of antimicrobial finishes on the biodeterioration of cotton and cotton/polyester fabrics: leaching versus bio-barrier formation. Polym Degrad Stab 96:1286–1296

Tshabalala MA, Kingshott P, VanLandingham MR, Plackett D (2003) Surface chemistry and moisture sorption properties of wood coated with multifunctional alkoxysilanes by sol-gel process. J Appl Polym Sci 88:2828–2841

Tsuboi M (1957) Infrared spectrum and crystal structure of cellulose. J Polym Sci 25:159–171

Valadez-Gonzalez A, Cervantes-Uc JM, Olayo R, Herrera-Franco PJ (1999) Chemical modification of henequén fibers with an organosilane coupling agent. Compos Part B Eng 30:321–331

Vasiljević J, Tomšič B, Jerman I, Orel B, Jakša G, Simončič B (2014) Novel multifunctional water- and oil-repellent, antibacterial, and flame-retardant cellulose fibres created by the sol–gel process. Cellulose 21:2611–2623

Vasiljević J, Jerman I, Jakša G, Alongi J, Malucelli G, Zorko M, Tomšič B, Simončič B (2015) Functionalization of cellulose fibres with DOPO-polysilsesquioxane flame retardant nanocoating. Cellulose. doi:10.1007/s10570-015-0599-x

Vilčnik A, Jerman I, Vuk AS, Koželj M, Orel B, Tomšič B, Simončič B, Kovač J (2009) Structural properties and antibacterial effects of hydrophobic and oleophobic sol–gel coatings for cotton fabrics. Langmuir 25:5869–5880

Vince J, Orel B, Vilčnik A, Fir M, Vuk AS, Jovanovski V, Simončič B (2006) Structural and water-repellent properties of a urea/poly(dimethylsiloxane) sol–gel hybrid and its bonding to cotton fabric. Langmuir 22:6489–6497

Vuk AS, Ješe R, Orel B, Dražič G (2005) The effect of surface hydroxyl groups on the adsorption properties of nanocrystalline TiO_2 films. Int J Photoenergy 7:163–168

Vuk AS, Ješe R, Gaberšček M, Orel B, Dražič G (2006) Structural and spectroelectrochemical (UV–Vis and IR) studies of nanocrystalline sol–gel derived TiO_2 films. Sol Energy Mater Sol C 90:452–468

Walrafen GE, Klein PH (1987) Infrared investigation of hydrogen-bonding on the surface of beryllium fluoride glass. J Chem Phys 86:6515–6522

Wang Z, Li G, Peng H, Zhang Z (2005) Study on novel antibacterial high-impact polystyrene/TiO_2 nanocomposites. J Mater Sci 40:6433–6438

Waschinski CJ, Tiller JC (2005) Poly(oxazoline)s with telechelic antimicrobial functions. Biomacromolecules 6:235–243

Xie YJ, Hill CAS, Xiao ZF, Militz H, Mai C (2010) Silane coupling agents used for natural fiber/polymer composites: a review. Compos Part A Appl Sci Manuf 41:806–819

Xue CH, Jia ST, Zhang J, Tian LQ (2009) Superhydrophobic surfaces on cotton textiles by complex coating of silica nanoparticles and hydrophobization. Thin Solid Films 517:4593–4598

Yun YJ, Chung JS, Kim S, Hahn SH, Kim EJ (2004) Low-temperature coating of sol–gel anatase thin films. Mater Lett 58:3703–3706

Zhu P, Sui SY, Wang B, Sun K, Sun G (2004) A study of pyrolysis and pyrolysis products of flame-retardant cotton fabrics by DSC, TGA, and PY-GC-MS. J Anal Appl Pyrolysis 71:645–655

Zollinger H (1991) Color chemistry: syntheses, properties and applications of organicdyes and pigments, 2nd edn. VCH Publisher, Weinheim/New York/Basel, Cambridge